Constructing ultra-permeable pillar[5]arene-based membrane with intramolecular water channels and precise molecular fractionation

Jinting Hu [a], Sem Bleus [b], Linde Achten [b], Yi Li [a], Samuel Eyley [c], Wim Thielemans [c], Ivo F.J. Vankelecom [d], Alexander Volodin [e], Wim Dehaen [b], and Xing Yang [a, *]

[a] Department of Chemical Engineering, KU Leuven, Celestijnenlaan 200F, B-3001 Heverlee, Belgium

[b] Sustainable Chemistry for Metals and Molecules, Department of Chemistry, KU Leuven, Celestijnenlaan 200F, B-3001 Leuven, Belgium

[c] Sustainable Materials Lab, Department of Chemical Engineering, KU Leuven, Campus Kulak Kortrijk, Etienne Sabbelaan 53, 8500 Kortrijk, Belgium

[d] Membrane Technology Group (MTG), Division cMACS, Faculty of Bio-Science Engineering, KU Leuven, Celestijnenlaan 200F, PO Box 2454, 3001 Leuven, Belgium

[e] Department of Physics and Astronomy, KU Leuven, Celestijnenlaan 200 D, B-3001 Leuven, Belgium

Corresponding author: X. Yang (xing.yang@kuleuven.be)

Abstract

Designing membranes with synthetic water channels has become an emerging topic to overcome the ubiquitous selectivity/permeability trade-off effect. In this study novel ultra-permeable thin film composite membranes with precise molecular fractionation were successfully fabricated. Per-hydroxylated pillar[5]arene (P[5]A), a macrocycle with a highly regular, cylindrical, angstrom-scale intramolecular cavity was applied as the aqueous monomer in interfacial polymerization (IP) to construct water channels in a thin film composite membrane. The competing effects of esterification and alkali-induced hydrolysis during IP were validated by investigating the effect of fabrication conditions. With almost complete rejection of model dyes >99.0% (*e.g.*, Congo Red & Direct Red 23) and low retention of salts (*e.g.*, 4.5% for NaCl & 18.9% for Na_2SO_4), the optimal membrane exhibited an ultra-high water permeance up to 267.1 $L \cdot m^{-2} \cdot h^{-1} \cdot bar^{-1}$, which is 3-10 times higher than most literature-reported membranes for similar applications. Also, the precision of dye/salt fractionation of the membrane was not affected by the increased feed salinity, with overall stable performance in 72h continuous operation. A high flux recovery of >94.5% proved that the membrane had low fouling propensity. Overall, the new route explored in this study provided inspiration for designing ultra-permeable membranes with precise molecular separation for environmental applications.

Keywords

Membrane filtration, water channel, per-hydroxylated pillar[5]arene, interfacial polymerization, dye/salt fractionation

1. Introduction

Membrane separation technology has rapidly developed and been applied in various fields such as water treatment, gas separation, energy storage, resource recovery, and other industrial production processes [1-3]. As an emerging technology, membrane separation has exhibited a tremendous application potential due to its advantages such as high versatility, reasonable energy consumption, small footprint, and easy scale-up [4, 5]. Nevertheless, the exploration for high-performance membranes with both high throughput and selectivity for target molecules is continuously ongoing, due to the ever-increasing environmental problems to be addressed and purification demands. Nowadays, to achieve near-zero discharge, novel membranes that can accurately harvest reusable resources from waste streams have drawn great interest [6].

Dye and salt ions are valuable resources that co-exist in most textile wastewater, while the disposal of their mixture is a major environmental challenge worldwide [7-9]. Large amounts of inorganic salts are added during the coloring process in order to accelerate the uptake of dyes by the textile, which makes the mixed wastes ecotoxic and not biodegradable [10, 11]. In addition, salts end up in the by-products of the dye synthesis processes, which makes it critical to harvest the high purity dye resource from the saline streams [12, 13]. Various robust methods such as adsorption, ion exchange, and advanced oxidation processes (AOPs) have been adopted to minimize the hazards of dye wastes to the ecosystem. Still, processes like adsorption and ion exchange require frequent regeneration [14-16]. AOPs may involve large chemical dosing and unidentified by-products [15, 17]. Furthermore, none of these processes can achieve satisfactory dye/salt fractionation for reuse. Membrane technology has also been adopted for dye wastewater treatment, but most commonly used nanofiltration (NF) membranes often reject simultaneously salt and dyes [18]. Most importantly, conventional NF can hardly provide a pure water permeance higher than 20 $L \cdot m^{-2} \cdot h^{-1} \cdot bar^{-1}$ ($LMH \cdot bar^{-1}$). Both low fractionation ability and low permeability have hindered further industrial adoptions [19, 20]. Thus, novel fabrication methods and membrane materials are highly sought after to construct new classes of membranes to

overcome the permeability-selectivity trade-off.

A thin selective layer with high porosity is crucial to achieve high permeability. Interfacial polymerization (IP) is a practical method to fabricate thin film composite (TFC) membranes on a robust supporting structure and a tunable selective skin layer [21]. By choosing from various monomers and adjusting the reaction conditions, membranes with target selectivity can be customized [22]. Although IP membranes with dense polyamide layers have demonstrated great potential in desalination [23-26], the design of polyester-based loose IP membranes recently drew attention with the advantage to push the permeability limit. Due to the lower reactivity of hydroxyl groups compared to amine groups in reaction with an acyl chloride, polyester-based thin films can exhibit a looser structure and hence are much more permeable than polyamides in most cases [27].

At the same time, numerous investigations have been conducted to improve membrane porosity [28, 29]. With the inspiration of biological proteins in cell membranes, macrocyclic molecules with intramolecular cavities have received increasing attention for the design of membranes with artificial water channels to increase membrane micro-isoporosity and overcome the selectivity/permeability trade-off [30, 31]. Annular molecules with angstrom-scale cavities, such as cyclodextrins (CDs), porous organic cages (*e.g.*, Noria) and cucurbiturils (CB), have been widely applied for membrane modification [32-35]. An IP membrane with cucurbit[6]uril (CB6) inclusions features enlarged polyamide tunnels due to the large steric hindrance of CB6, resulting in a fourfold enhanced water permeability compared to unmodified membranes, while maintaining high Na_2SO_4 rejection [32]. A CB6-embeded polyamide membrane on a patterned substrate achieved a high water permeability of 124.9 $LMH \cdot bar^{-1}$ and a rejection of 99.9% for Janus Green B [36]. Thus, utilizing monomers with well-defined cavities can be an attractive route for developing membrane with high permeability. Nevertheless, both suitable macrocyclic monomers and fabrication methods need to be explored.

Pillar[n]arenes are supramolecular macrocyclic molecules first reported in 2008

[37]. With the methylene bridges linked in the para-position in between hydroquinone or dialkoxybenzene units, pillar[n]arenes demonstrate symmetrical pillar architectures and rigid electron-rich cavities [38, 39]. Since their discovery, pillar[n]arenes immediately attracted great attention in host–guest chemistry, supramolecular chemistry, smart materials, and transmembrane channels [40-43]. Efforts have been made to utilize pillar[5]arene cavity to boost the membrane water permeability, *e.g.*, a polymer bilayer membrane incorporated with peptide-appended pillar[5]arene achieved nearly 10 times more water conductive than commercial NF [44-46]. Pillar[n]arene derivatives were also constructed into artificial channels for transporting solutes (*e.g.*, protons and ions) [42]. Although proposed in several as-mentioned studies, the hypothesis of water conductivity of pillar[5]arene when embedded into membrane matrix was not proved. So far only a handful of studies validated the feasibility of combining pillar[n]arene *via* the IP method for fabricating organic solvent filtration membranes [47, 48]. However, regardless of the fabrication means, none of the above-mentioned studies has comprehensively explored the mechanism of pillar[n]arene layer formation, including in IP. Thus, there is a general lack of understanding on the correlation between the fabrication conditions and filtration behavior of pillar[n]arene membrane .

In this study, a new class of pillar[n]arene-based membranes is developed *via* the IP method, incorporating per-hydroxylated pillar[5]arene (P[5]A) monomers with the aim of constructing thin film composite (TFC) membranes with ultra-thin and ultra-permeable selective layers. The mechanisms of IP layer formation are explained through investigation of the membrane properties obtained under different IP conditions. The membrane performance is further tested for dye/salt fractionation using simulated textile wastewater with various compositions. As illustrated in **Fig. 1**, under suitable IP conditions the phenolic hydroxyls of P[5]A in the aqueous phase are reactive towards acyl chloride groups of cross-linkers in the organic phase, which results in the formation of the polyester layer. It is hypothesized that the low reactivity of phenolic hydroxyls and the steric hindrance of P[5]A macrocycles can act synergistically to build a loose

pore structure in the selective layer; while the unreacted hydroxyl groups can contribute to membrane hydrophilicity, rendering the membrane highly permeable to water and resistant to hydrophobic foulants [23, 49]. Moreover, the P[5]A intramolecular cavity, with a reported diameter of 4.7Å, is expected to enrich the membrane nano-isoporosity significantly [43]. These novel P[5]A-TFC membranes are designed to overcome the selectivity/permeability trade-off effect and achieve efficient molecular fractionation.

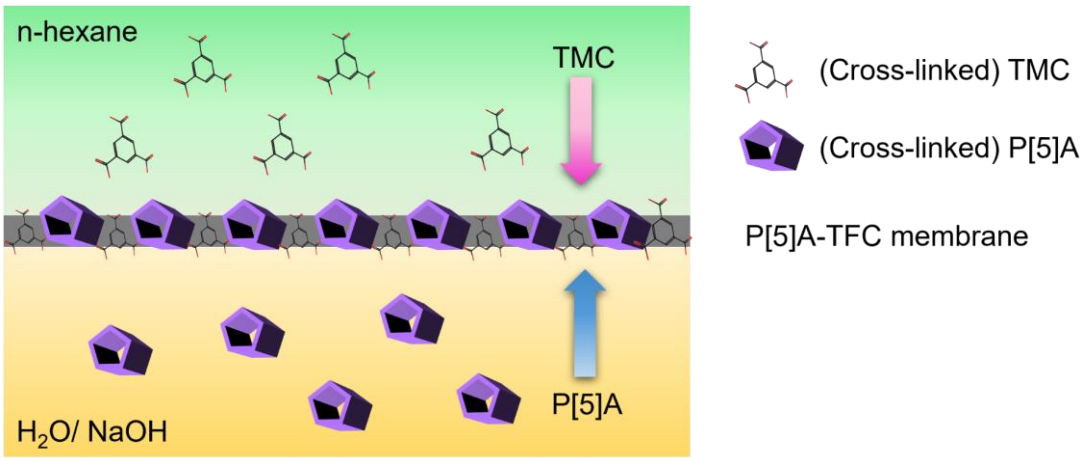

Fig. 1. The formation of P[5]A-TFC membrane *via* IP process.

2. Experimental

2.1. Materials and chemicals

Polypropylene/Polyethylene (PP/PE) non-woven fabric (Novatexx 2471) was acquired from Freudenberg Filtration Technologies, Germany. Polyether sulfone (PES) in the form of powder (Veradel® 3000P) was purchased from Solvay S.A. Unless otherwise specified, all the other chemicals were purchased from Sigma-Aldrich and used without further purification. Detailed information is shown in **Section S1** in the Supplementary Information (SI).

2.2. Synthesis of pillar[5]arene (P[5]A) monomers

Per-hydroxylated pillar[5]arene (P[5]A) with a molecular weight (MW) of 610.6 g/mol and its precursor per-methoxypillar[5]arene were synthesized by adapting established methods [50, 51], the detailed procedures of which are shown in the **Section S2** in the SI.

2.3. Preparation of PES substrate and P[5]A-TFC membranes

The PES membrane substrates were prepared *via* the non-solvent induced phase inversion (NIPS) method [52, 53]. Detailed procedures are provided in **Section S3**.

As shown in **Fig. 2**, the P[5]A-TFC membranes were fabricated *via* an IP reaction that took place on the PES substrate surface, between the P[5]A monomers in the aqueous phase and TMC monomers in the organic phase. Detailed procedures are provided in **Section S3**.

A series of P[5]A-TFC membranes were synthesized by varying the dosage of P[5]A monomers (*i.e.*, 1.2 to 1.8 wt%) and NaOH (*i.e.*, 0.3 to 0.7 wt%) in the aqueous phase, as well as the IP reaction time (*i.e.*, 1 to 5 min). Those membranes were labeled as P*xx*N*xx*IP*x*, as listed in **Table 1**. The first and second '*xx*' represent the concentration of P[5]A and NaOH, respectively, and the last '*x*' refers to the IP reaction time applied. The pristine PES membrane with 15 wt% polymer concentration served as substrate and was also tested as a benchmark for performance.

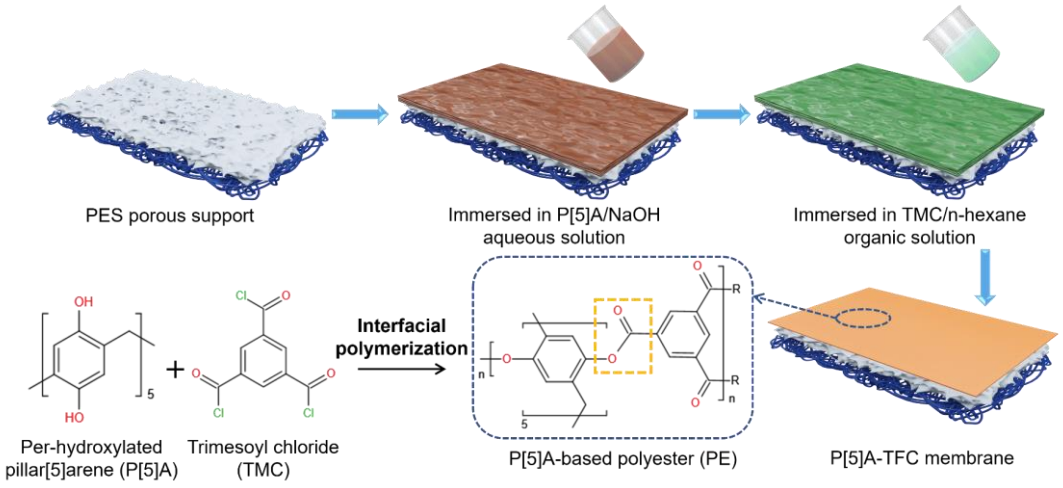

Fig. 2. Scheme of the fabrication process and IP reaction mechanism for the P[5]A-

TFC membrane.

Table 1. IP parameters for P[5]A-TFC membranes (with constant organic phase composition of 0.2 wt% TMC in n-hexane)

	P[5]A dosage, wt%	NaOH dosage, wt%	IP reaction time, min
PES15 substrate	—	—	—
P1.2N0.5IP1	1.20	0.5	1
P1.35N0.5IP1	1.35	0.5	1
P1.5N0.5IP1	1.50	0.5	1
P1.65N0.5IP1	1.65	0.5	1
P1.8N0.5IP1	1.80	0.5	1
P1.5N0.3IP1	1.50	0.3	1
P1.5N0.4IP1	1.50	0.4	1
P1.5N0.6IP1	1.50	0.6	1
P1.5N0.7IP1	1.50	0.7	1
P1.5N0.5IP3	1.50	0.5	3
P1.5N0.5IP5	1.50	0.5	5

2.5. Preliminary filtration performance evaluation

The membrane filtration performance was evaluated in terms of water permeance and rejection of various solutes with single solute solutions, *i.e.,* single salt solution (NaCl, Na_2SO_4 1000 ppm) and singe anionic dye solution (Congo Red (CR), Direct Red 23 (DR23), Reactive Blue 2 (RB2) and Direct Red 80 (DR80), 200 ppm). While all the tests were done with anionic dyes, an additional test with a cationic dye Methylene Blue (MB) was briefly demonstrated with the selected membrane P1.5N0.5IP1. Detailed procedures and indices are described in **Section S4**.

2.6. Dye/salt fractionation and long-term stability tests

The optimal membrane (*i.e.*, P1.5N0.5IP1) was selected based on experiments in **Section 2.5** to carry out the dye/salt fractionation tests. Dye solutions (200 ppm DR23)

mixed with varying concentration of salt (0 – 40 g/L Na_2SO_4) were applied as the feed solution. Furthermore, the long-term stability tests of the optimal membrane were conducted with a mixed solution containing 200 ppm DR23 and 1 g/L Na_2SO_4. Detailed procedures are described in **Section S5**.

2.7. Fouling experiments

Three dyes (CR, DR23, RB2) were selected as the respective model foulant to investigate the anti-fouling performance of the P[5]A-TFC membranes in a 2-cycle experiment. Each solution contained 200 ppm single dye and served as the feed stream in the cross-flow apparatus at room temperature and TMP of 2 bar. Fouling indices including the flux recovery ratio (*FRR*), the total fouling ratio (R_t), the reversible fouling ratio (R_r), and the irreversible fouling ratio (R_{ir}) were analyzed accordingly to evaluate the membrane anti-fouling performance. The experimental steps of each cycle and the calculating equations are briefly described in **Section S6**.

In general, a higher FRR and a lower R_t indicate better anti-fouling behavior of the membrane [54]. The R_r is usually related to the flux drop caused by concentration polarization and the formation of loosely attached filtration cake, whereas R_{ir} represents the adsorption of foulants which cannot be removed easily [55].

All characterization methods involved in the above experiments, *i.e.*, P[5]A monomers, membrane morphological and surface chemical composition, molecular-weight-cut-off (MWCO) of the membrane using Polyethylene glycols(PEG), solution properties, are described in **Section S2, Section S7 and Section S8**.

3. Results and discussion

3.1. Surface chemistry of P[5]A-TFC membranes

After confirming the successful synthesis of the P[5]A monomer based on the nuclear magnetic resonance spectrum (NMR) results presented in **Fig. S2**, **Fig. S3** and **Fig. S5**, **Fig. S6** in the SI, further investigations on the surface chemical composition

of the as-prepared P[5]A-TFC membranes were conducted *via* Fourier-transform infrared spectroscopy (FT-IR) and X-ray photoelectron spectroscopy (XPS). As presented in the FTIR spectrum in **Fig. 3a**, after eliminating the characteristic peaks of the PES substrate *via* background subtraction, the P1.5N0.5IP1 membrane (green line) shows distinct absorption bands at around 1700 cm^{-1}, 1750 cm^{-1} and between 3000 cm^{-1} - 3500 cm^{-1}, which can be attributed to the existence of C=O groups and -OH groups, respectively. Here the C=O stretching around 1700 cm^{-1} and 1750 cm^{-1} could be associated with two sources, *i.e.*, the ester C=O and/or the carboxylic C=O (carboxylic acid and/or sodium carboxylate) [56]. The former indicates that the esterification successfully took place between the hydroxyl groups of P[5]A and acyl chlorides of TMC; whereas the potential presence of the carboxylic acid C=O could be attributed to the hydrolysis of unreacted acyl chlorides [57]. The broad characteristic peak of -OH groups between 3000 cm^{-1} and 3500 cm^{-1} may be attributed to residual unreacted hydroxyl groups and hydrolyzed acyl chlorides, considering the relatively low reactivity of the phenolic hydroxyls and the steric hindrance of P[5]A macrocycles that could have led to an incomplete IP reaction.

The XPS results of the selected membranes are presented in **Fig. 3b-c**, which show the deconvoluted C 1s spectra of the respective PES substrate and the P[5]A-TFC membrane surface. Compared to the PES, the P1.5N0.5IP1 membrane displays new $^{-}$O-C=O, and RO-C=O contributions (brown and blue peaks), which is in good agreement with the FT-IR results. Similar new peaks were also observed on other P[5]A-TFC membranes as presented in **Figure S8**. Due to changes in synthesis conditions, the new peaks presented different intensities. To better understand these differences, the homogeneous equivalent elemental compositions of selected membranes were determined from the XPS survey spectra, as presented and summarized in **Fig. 3d** and **Table S2**. With an analysis area of 700 μm × 300 μm per measurement, XPS results are able to reveal the surface coverage uniformity by detecting the residue sulfur content from the PES substrate, especially when the polyester layer is thin and patchy. It can be concluded that membranes P1.5N0.5IP5 and

P1.65N0.5IP1 have the highest polyester coverage, whereas membranes P1.35N0.5IP1 and P1.5N0.6IP1 have the lowest. The rest of the samples presented a similar sulfur content. This phenomenon could be explained *via* decreased polyester layer thickness or decreased homogeneity of the IP layer, which will be explained in the following **Section 3.2**. Combining the above-mentioned results, it can be confirmed that the P[5]A-based polyester skin layer was successfully synthesized on the surface of the PES substrate.

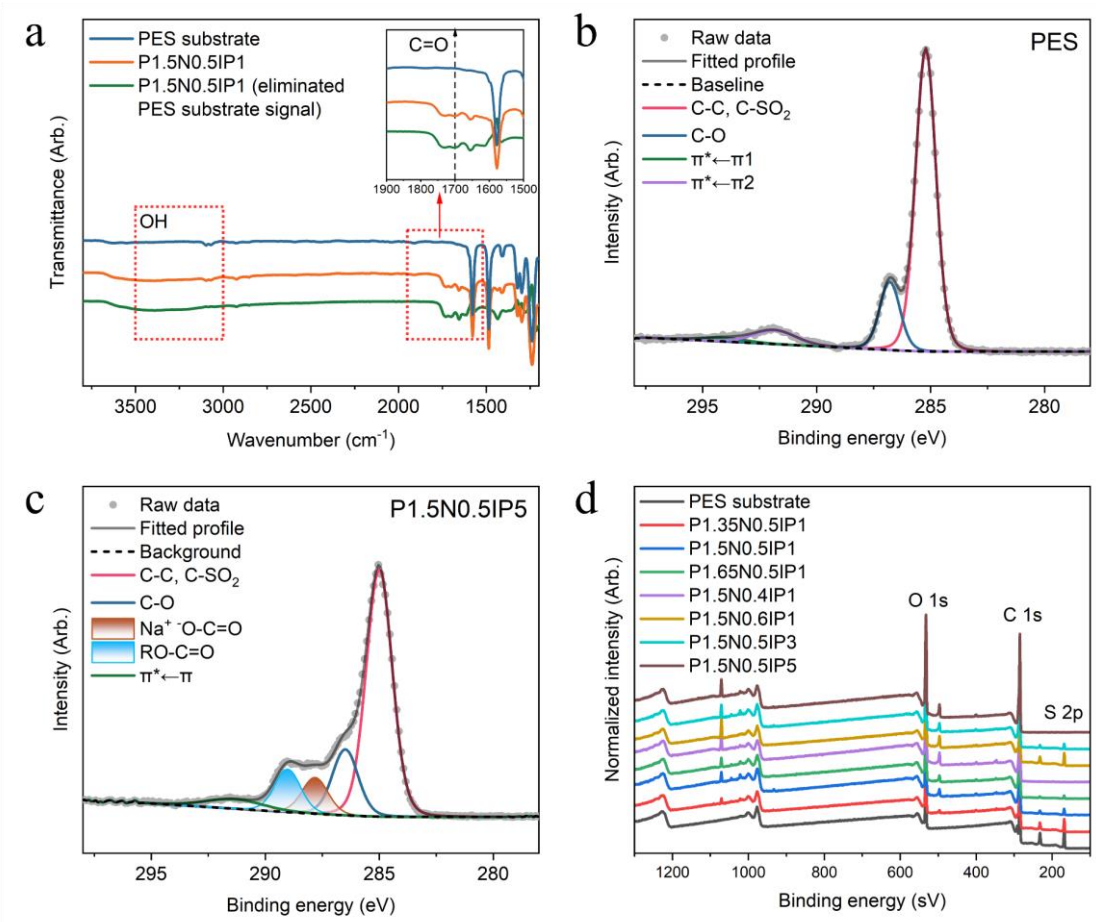

Fig. 3. Chemical characterization of PES substrate and P[5]A-TFC membranes. (a) The FT-IR spectrum of PES substrate, P1.5N0.5IP1 and P1.5N0.5IP1 after eliminating PES substrate signal; (b) The C 1s spectra of PES substrate; (c) The C 1s spectra of P1.5N0.5IP1; (d) The XPS survey spectra of PES substrate and P[5]A-TFC membranes.

3.2. Surface morphology of P[5]A-TFC membranes

The surface morphological changes of the P[5]A-TFC membranes, as compared to those of the pristine PES were revealed using scanning electronic microscopy (SEM). **Fig. S9** shows that the obtained PES substrate structure shows good agreement with reported work [58]. The effect of the IP reaction time was evaluated by keeping the rest of the experimental conditions constant, such as the respective P[5]A and NaOH dosage. As presented in **Fig. 4(a-c)**, with the increase in IP time from 1 to 5 min, the appearance of the membrane surface transformed from being uniform and smooth, to having a deflated-bubble-like structure and typical stacking Turing patterns [59]. Numerous studies proved that the formation kinetics of the IP layer is greatly influenced by the diffusion of monomers and hindered by the self-limiting tendency of the IP reaction [60]. In short, the MW of polyester increases up to the phase separation value in a very short time (< 1 s) after the two phases come into contact causing the polyester chains to precipitate from the organic phase. Then, due to the formation of the crosslinked polymer network, liquid–liquid diffusion gradually transitions to selective diffusion through the newly-formed polyester layer. Therefore, the diffusion resistance will continuously increase with the increasing crosslinking degree (higher polyester MW and density), namely the self-limiting nature of the IP reaction. Thus, it can be considered that the typical stacking structure was formed during the self-limiting diffusion of the IP reaction. Eventually, the polymerization degree will reach a stable state and the IP reaction will terminate. Consistently, the atomic force microscopy (AFM) images of these three membrane samples showed that the surface becomes rougher due to the more significant ridge-and-valley structures at increased IP times. The observations are further confirmed by the cross-sectional morphology of P[5]A-TFC membranes in **Fig. 4(d-f)**, which shows that the thickness of the selective layer increased with increasing IP reaction time.

Similar results were observed with the membranes synthesized at varying P[5]A dosage, where the NaOH dosage of 0.5 wt% and IP time of 1 min were kept constant. As presented in **Fig. S10 (a-c)** in SI, when the P[5]A monomer dosage was lower than

1.5 wt%, the membrane surface was relatively smooth. When the P[5]A monomer dosage was increased to 1.65 wt%, similar surface stacking patterns to those in **Fig. 4 (b & c)** appeared. Thus, the increased concentration of P[5]A can strongly accelerate the diffusion and polymerization, which eventually shaped this similar stacking surface. Increased surface roughness can also be seen in the AFM images of P[5]A-TFC membranes with increasing P[5]A dosage in **Fig. S10 (d-f)**, proving that a higher polymerization degree resulted in a rougher membrane surface, which is consistent with the findings in other work [61, 62]. The increased IP layer thickness with increasing P[5]A dosage in **Fig. S10 (g-i)** further confirmed the difference in polymerization degree. The SEM results in **Fig. S11** show the surface morphology of P[5]A-TFC membranes with varying NaOH dosage from 0.4 to 0.6 wt%, at constant P[5]A dosage of 1.5 wt% and IP time of 1 min. It is interesting to observe that the ridges and valleys became more prominent with increasing NaOH dosage, proving that NaOH can promote the esterification process. It is also worth noting that the stacking pattern on the surface of P1.5N0.6IP1 widened and became less distinct, which might be a consequence of NaOH-induced alkali hydrolysis (to be discussed in **Section 3.4.1**). Overall, the initial P[5]A concentration, NaOH dosage, and IP time contributed synergistically to shape the membrane morphology. Well-controlled synthesis conditions can be beneficial to fabricate a thin and homogenous selective layer of the TFC membrane, *e.g.*, moderate P[5]A concentration of 1.5 wt%, NaOH dosage of 0.5 wt%, and a short IP time (1 min).

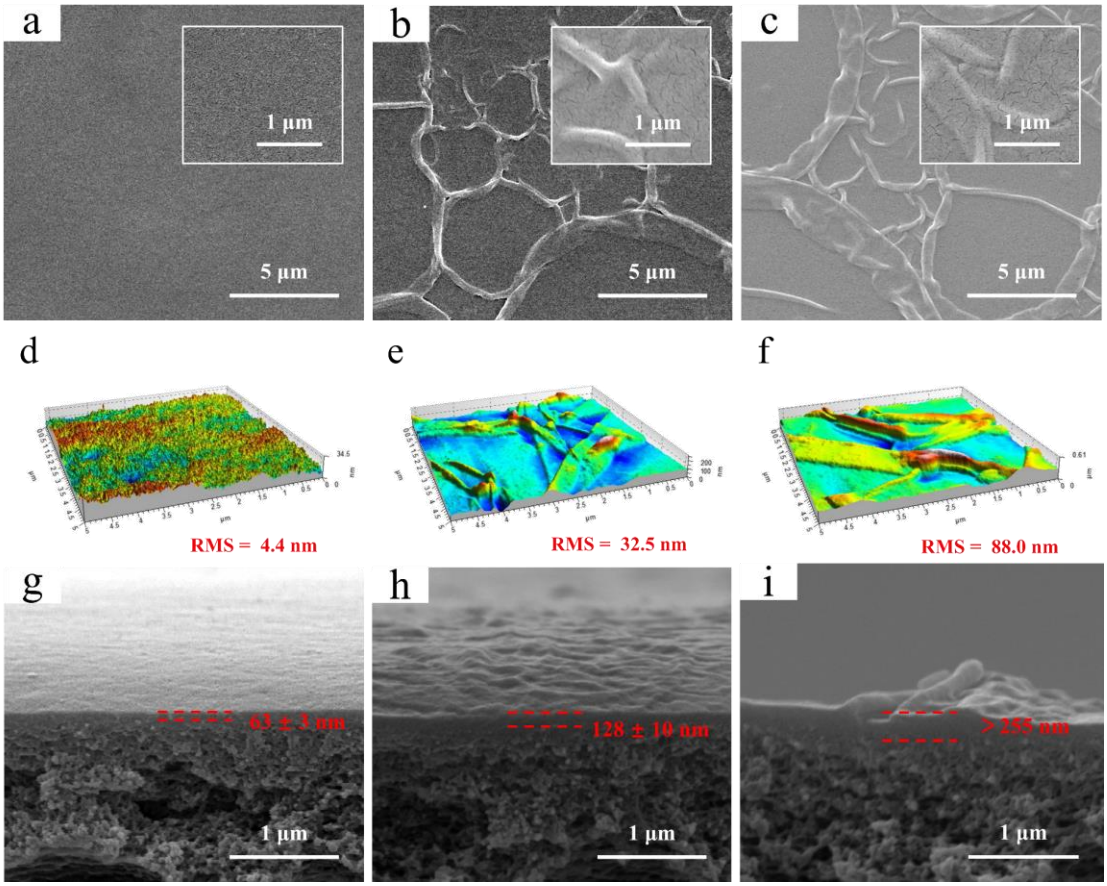

Fig. 4. The surface morphology of P[5]A-TFC membranes by varying the IP reaction time (a) P1.5N0.5IP1, (b) P1.5N0.5IP3, (c) P1.5N0.5IP5, (SEM images); the AFM images and the RMS roughness of (d) P1.5N0.5IP1, (e) P1.5N0.5IP3, (f) P1.5N0.5IP5; cross-sectional morphology of (g) P1.5N0.5IP1, (h) P1.5N0.5IP3, (i) P1.5N0.5IP5.

3.3. Surface hydrophilicity and charge characteristics of P[5]A-TFC membranes

Fig. 5a presents the water contact angle (WCA) results of the P[5]A-TFC membranes. It was found that the pristine PES membrane demonstrated a slight hydrophilic surface with a WCA of 67.1°. After the IP reaction, the P[5]A-TFC membranes exhibited enhanced hydrophilicity with lower WCAs in the range of 30~55°. The increased hydrophilicity can be explained by the enrichment of hydrophilic groups such as the unreacted hydroxyls from P[5]A after the IP reaction and the carboxylic acid groups generated by the acyl chloride hydrolysis [63]. As reported, the membrane anti-fouling behavior is closely related to the wettability of the membrane surface [64].

Benefiting from the hydration layer formed by the interactions between surface hydrophilic groups and surrounding water molecules, the deposition and adsorption of hydrophobic foulants is greatly weakened [65, 66]. Moreover, introducing hydrophilic groups can also improve the water permeability of the membrane [67, 68].

The ζ-potential results of the pristine PES substrate and a representative P[5]A-TFC membrane, *i.e.*, P1.5N0.5IP1, P1.5N0.5IP3, P1.5N0.5IP5, are presented in **Fig. 5b**. After being coated with a P[5]A-based polyester thin film, the P1.5N0.5IP1 membrane demonstrated an enhanced negative charge over a wide pH range (4.5 – 10.5) compared to the pristine PES. These changes might be attributed to the presence of hydrolyzed acyl chlorides[63]. The surface charge holds vital significance in the electrostatic interactions between the surface and charged solutes. Thus, with the highly negatively charged surface, the prepared P[5]A-TFC membranes are expected to have a higher rejection of anionic molecules and may also possess anti-fouling properties when in contact with negatively charged foulants [69].

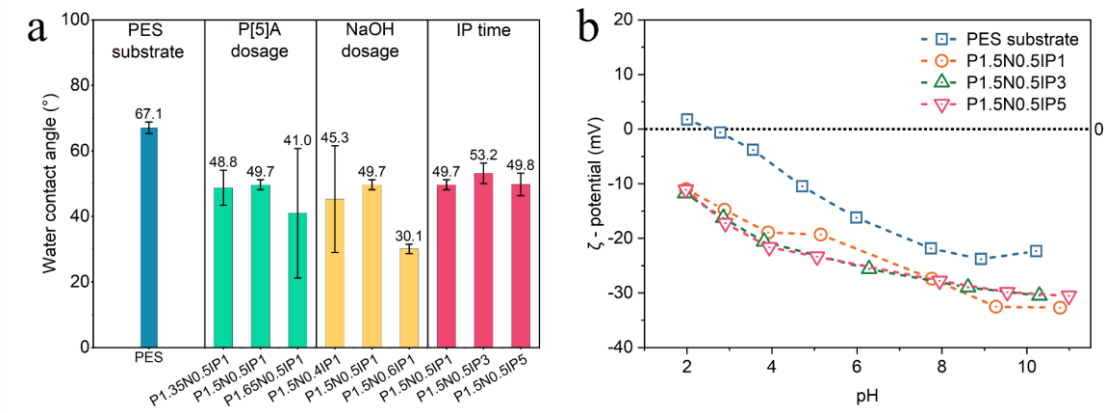

Fig. 5. (a) Water contact angles of PES substrate and P[5]A-TFC membranes; (b) ζ-potentials of PES substrate and P1.5N0.5IP1, P1.5N0.5IP3, P1.5N0.5IP5 membranes.

3.4. Filtration performance of P[5]A-TFC membranes

3.4.1. Pure water permeance of P[5]A-TFC membranes

Fig. 6 shows the comparison of the permeance of the P[5]A-TFC membranes when using DI water and salt solutions containing NaCl and Na_2SO_4, respectively, at different

concentrations of P[5]A monomer (**Fig. 6a**), different dosages of NaOH (**Fig. 6b**), and various IP reaction times (**Fig. 6c**). One synthesis parameter was varied at a time while the others were kept constant. Here the water permeance of the PES substrate was used to benchmark the performance of the TFC membranes (**Fig. S13**), the PES membrane showed significantly higher pure water permeance (889.5 LMH·bar^{-1}) than the TFC membrane ones. This serves as a good indication that a surface layer has been formed on the TFC membranes. The results are in good accordance with the cross-section SEM images in **Section 3.2** and **3.3**, where the presence of a selective layer on the TFC membranes was identified after the IP reaction.

Firstly, we will discuss the base case, *i.e.*, pure water permeance with DI water (as blue bars) for varying membrane synthesis conditions. It can be seen from **Fig. 6a**, at constant NaOH dosage and IP time, the membrane water permeance decreased from 317.1 to 118.6 LMH·bar^{-1} at increasing dosage of P[5]A from 1.2 wt% to 1.8 wt%. This phenomenon is consistent with the change in membrane surface morphology (**Fig. S10 (g~i)**), which showed that a significant increase in membrane thickness corresponded to an increase in P[5]A concentration. Thus, it is likely that the enrichment of P[5]A monomer in the aqueous solution greatly accelerated its diffusion towards the IP interface and then further accelerated the IP reaction within a limited phase contact time, resulting in a higher cross-linking degree and thicker polyester layer [70].

The opposite was observed for the permeability changes occurring when increasing the NaOH dosage in the aqueous phase. As presented in **Fig. 6b**, the pure water permeance (blue bars) increased slightly when the NaOH dosage increased from 0.3 to 0.5 wt%, and it dramatically surged nearly two-fold with a further increase of NaOH dosage beyond 0.6 wt%. Traditionally, NaOH is widely applied in surface modification of polyester materials as it can induce hydrolysis of ester groups [71-73]. The increasing permeance at increased NaOH dosage again proves our hypothesis that simultaneous nucleophilic substitution and hydrolysis reactions, which hydrolyze the newly formed ester bonds into hydroxyl and carboxylic end groups, might have happened during the IP cross-linking reactions [71]. As a result, the formation of a loose

pore structure in the IP layer was achieved, leading to increased water permeance. Nevertheless, with a further increase of NaOH beyond 0.5 wt%, the alkali hydrolysis reaction starts to play a dominant role in the esterification-hydrolysis equilibrium, which would further loosen the pore structure and may compromise the rejection of solutes (will be discussed in **Section 3.4.2** and **Section 3.4.3**).

As shown in **Fig. 6c**, the IP reaction time also plays a critical role in determining the water permeability. By extending the reaction time from 1 to 3 min, a permeance decrease was observed as expected, while a further time extension to 5 min led to a slight increase in permeance. This is because of the two competing mechanisms of esterification and hydrolysis as illustrated in **Section 3.2**. The IP reaction is a self-limiting process, which means the newly generated cross-linked structure will increase the resistance to monomer diffusion [74], causing the esterification process to slow down. Meanwhile, the ongoing alkali hydrolysis will gradually break down the ester links. For short IP times (< 3min), the IP reaction is sufficiently fast and hence its densification effect due to esterification will be dominant, causing the water permeability to decrease. When the IP time exceeds a certain limit (*e.g.*, 5 min in this study), the hydrolysis will be more dominant and hence start to loosen the pore structure. This trend with increasing IP time observed here is consistent with those reported in the literature [62].

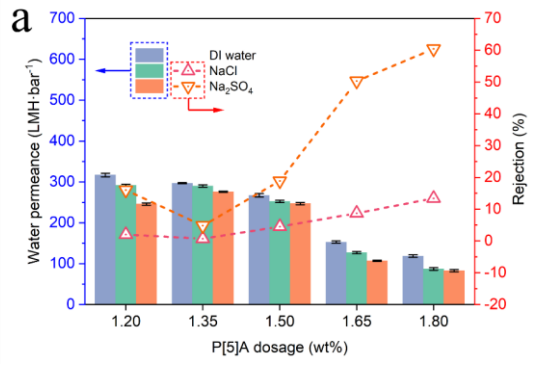

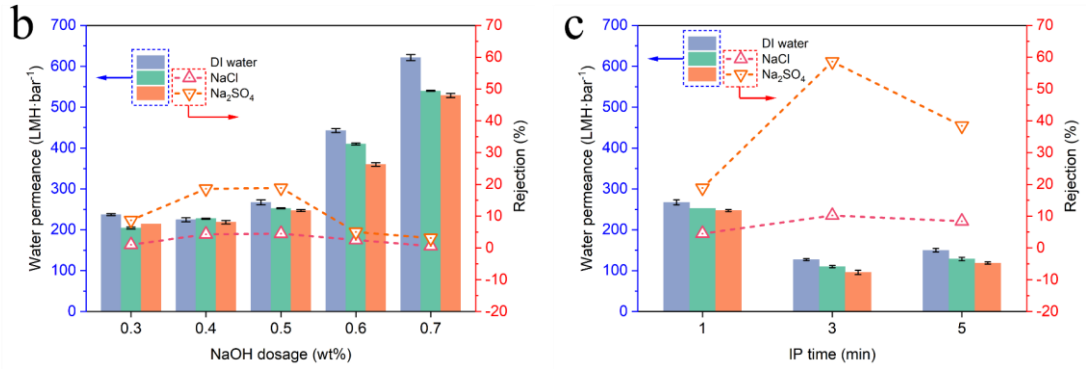

Fig. 6. Pure water permeance, salt solution permeance and salt rejection of P[5]A-TFC membranes with (a) different P[5]A monomer dosages in aqueous solution; (b) different NaOH dosages in aqueous solution; and (c) different IP reaction times. Each simulated feed contained single salt of either NaCl or Na_2SO_4 in 1000 ppm. (applied pressure in cross-flow: 2 bar; benchmarking synthesis conditions: P[5]A 1.5 wt%, NaOH 0.5 wt%, and IP time 1 min).

3.4.2. Salt rejection of P[5]A-TFC membranes

The results of the salt solution filtration tests in terms of the permeance and solute rejection are also summarized in **Fig.6**, with simulated feed solution with single solute of either NaCl (green bars and pink dash lines) or Na_2SO_4 (orange bars and dash lines). As compared to the pure water permeability, the permeance of salted feeds follows the same trend at varying fabrication conditions (*i.e.*, P[5]A concentration, NaOH dosage, IP time), but overall lower (2-30%) in magnitude. In general and within experimental error, for each fabrication condition the water permeance follows a similar decreasing order of pure water > NaCl solution > Na_2SO_4 solution. The decrease is likely due to the increase of the osmotic pressure of the feed, and effects of concentration polarization at the boundary layer adjacent to the membrane surface [75].

The discussion below will mainly focus on the rejection of solutes to highlight the influence of the fabrication conditions. As presented in **Fig. 6a**, at low P[5]A concentration in the aqueous phase (up to 1.5 wt%), the rejection values of these

membranes for NaCl and Na_2SO_4 are lower than 4.5% and 18.9%, respectively, which indicate a high salt permeation. However, when further increasing the P[5]A concentration beyond 1.65 wt%, the NaCl rejection increases up to 13.4% and the Na_2SO_4 rejection increases sharply up to 60.4%. The rejection results were also in agreement with the changes of membrane morphologies presented in **Fig. S10 (a~c)**, where a transition from smooth (P[5]A concentration up to 1.5 wt%) to stacking pattern surface (beyond 1.5 wt%) was observed at increasing P[5]A concentration; meanwhile the thickness of the IP layer also increased accordingly. Therefore, all these observations were consistent with the increasing trend of salt rejection results.

It can be seen from **Fig. 6b**, the salt rejection of the P[5]A-TFC membranes prepared at increasing dosage of NaOH demonstrated firstly an increasing and then a decreasing trend, *i.e.*, by increasing the NaOH dosage in the low range, the rejection of Na_2SO_4 firstly increases slightly from 8.7% at 0.3 wt% NaOH, to 18.9% at 0.5 wt% NaOH; a further increase of the NaOH dosage leads to a sharp decline of rejection to 3.1%. The rejection of NaCl shows a similar trend but remains overall low (< 5.0%) throughout the range of NaOH wt%. The slight increase of solute rejection at the low dosage range (*i.e.*, ≤ 0.5 wt%) proved that a certain dosage of NaOH can boost the IP cross-linking reaction and produce a denser IP layer. As explained in **Section 3.4.1**, the competition between the cross-linking reaction (*i.e.*, esterification) and NaOH induced alkali hydrolysis during the IP process will determine the permeability – rejection behavior of the membrane. Overdosing NaOH likely causes the latter to become dominant and produce a looser pore structure, leading to greatly enhanced permeabilities for both salt ions and water.

As shown in **Fig. 6c**, the IP reaction time also plays a critical role in membrane rejection and permeability of salt solutions. While the membrane water permeance for salt solution follows the same trend as that of pure water (**Section 3.4.1**), the rejection of Na_2SO_4 increases significantly from 18.9% to 58.6% and for NaCl also increases from 4.5% to 10.2% with increasing IP time from 1 to 3 min; While further increasing the IP time to 5 min, the respective rejection for Na_2SO_4 and NaCl drop to 38.4% and

8.4%. As explained in **Section 3.4.1**, the reason is mainly attributed to the self-limiting nature of the IP and the competing effect of the alkali hydrolysis with the presence of NaOH. Therefore, an appropriate IP time should be chosen based on the separation target, for example, if the target is to have both high water and salt permeability, a low IP time should be chosen, which reaches good agreement with the morphological analysis (**Section 3.2**).

It is worth noticing that for all membranes tested, the trend of salt ion rejection was synchronized with the changes in permeability, *e.g.*, a higher permeance is accompanied with a lower salt rejection, reflecting the classical permeability – rejection trade-off. This trend proves that the denser structure was attributed to an enhanced cross-linking degree during IP, resulting in a higher resistance to the passage of salt ions. Furthermore, the rejection of SO_4^{2-} salt fluctuated much more intensely than that of Cl^- one. As for charged nanofiltration membranes, the main rejection mechanisms can be attributed to the steric hindrance, Donnan equilibrium and dielectric exclusion [76, 77]. Thus, compare to monovalent ions such as Cl^-, the rejection trend divalent ions such as SO_4^{2-} with stronger charge and larger hydrated ionic size tend to be more sensitive to the changes in membrane pore structure and surface charge [78].

3.4.3. Dye rejection of P[5]A-TFC membranes

With simulated dye solutions as feeds, the filtration performance of the P[5]A-TFC membranes as a function of different synthesis conditions is presented in **Fig. 7**. Clearly, with the increases of P[5]A dosage from 1.2 to 1.8 wt % in the membrane, the rejection of all anionic dyes increases, *e.g.*, for CR increasing from 98.0 to 99.8 %, DR23 increasing from 98.1 to 99.5 %, RB2 increasing from 96.9 to 99.7 %, and DR80 from 98.6% to 100%, respectively. However, within the experimental error, the overall trend of permeance decreases slightly with increasing P[5]A dosage at the low range (*i.e.*, 1.2 ~ 1.5 wt%), but remains within the range of 205-280 $LMH \cdot bar^{-1}$ with all simulated dye solutions; while a significant decrease occurs when increasing the dosage further. The lowest permeance of 70 $LMH \cdot bar^{-1}$ was observed at a P[5]A dosage of 1.80

wt% with the DR80 solution. The overall trend in permeance at varying P[5]A dosage is consistent with that observed for the pure water permeance (**Fig. 6a**). The dye rejection results are in good agreements with that of the salt ions, as well as the analysis of the membrane surface morphologies (**Fig. S10**) in **Section 3.2**. In brief, the increased initial dosage of P[5]A monomer possessed higher monomer diffusion rate, which resulted in a thicker and denser polyester selective layer under the same reaction time. The thicker IP layer guaranteed a high rejection for all model dye solutes, however with a compromise in the membrane permeability. However, the overall excellent performance of high permeability and dye rejection of the as-developed TFC membranes can also be attributed to the enhanced negative surface potential and hydrophilic surface properties of the membrane, which are consistent with the surface characterization results in **Section 3.3**.

When benchmarking with the PES substrate, the dye rejection performance of P[5]A-TFC membranes are greatly enhanced. For example, the dye rejection rate of P1.5N0.5IP1 increased from 89.5 to 99.7% for CR and 90.8 to 99.4% for DR23; the rejection rate of RB2 increased dramatically from 62.2 to 99.0%. These results are in good accordance with the ζ-potential and MWCO characterization (**Fig. 5b**, **Fig. S12**), the IP reaction indeed created a denser membrane surface with enhanced negative charge, which allows the P[5]A-TFC membrane to screen out target dye solutes. In addition, a preliminary test with a cationic dye MB containing feed solution (results shown in **Fig. S14**) proved that the membrane P1.5N0.5IP1 demonstrated 110.0 $LMH \cdot bar^{-1}$ water permeance and 37.8% MB rejection. Although MB has lower molecule weight, the permeance decrease with MB solution is more significant than those with selected anionic dyes. Compared to the membrane after anionic dye (CR) filtration, which showed intactness of the effective membrane area (**Fig. S15c**), significant adsorption of MB was observed on the membrane surface (**Fig. S15b**). The phenomenon can be explained *via* the negatively charged nature of the membrane surface (**Fig. 5b**). With the main aim to investigate the membrane formation mechanism in this study, the membrane performance will be mainly evaluated *via* anionic dyes

based on the characteristics of the as-developed membranes.

As revealed in **Fig. 7b**, in the low dosage range of NaOH, *i.e.*, 0.3 to 0.5 wt%, the rejection for all dyes increases with increasing NaOH concentration, for example, the rejection of DR23 increased from 98.5 to 99.4%, and the rejection of RB2 increased from 91.7 to 99.0%. This is due to the promotion of the IP reaction and hence a higher cross-linking degree at the selective layer of membrane. Nevertheless, a further increase of NaOH to 0.6 and 0.7 wt% would lead to a loss of the dye rejection. For example, the rejection of DR23 changed from 99.4% (at 0.5 wt% NaOH) to 98.1% (at 0.7 wt% NaOH); while the rejection of RB2 decreases sharply from 99.0% (at 0.5 wt% NaOH) to 81.1% (at 0.7 wt% NaOH), indicating that almost 20% RB2 leaked into the permeate side. The results are consistent with the observation in the salt rejection in **Fig. 6b**, and can also be explained *via* the competing effect of the hydrolysis reaction at high NaOH dosage. Although also being an anionic dye, it is interesting to note that the rejection for RB2 (774.2 Da) is generally the lowest for all tests, and it changes much more dramatically than dye ions with similar (DR23, 813.7 Da) or even smaller size (CR, 696.7 Da). This is due to the smaller aggregation degree of reactive dyes than that of direct dyes, so RB2 turned to be more dispersed as smaller particles in the aqueous solution; whereas those direct dye molecules were inclined to form aggregates/clusters with enlarged effective size during filtration [79-81]. Similar changes can also be found in **Fig. 7c**, with the prolonged IP reaction time, the P[5]A-TFC membranes turned to be firstly denser (from 1 to 3 min) then became looser (from 3 to 5 min) due to the competing effects of esterification and hydrolysis reaction, as explained in detail in **Section 3.4.1**. This hypothesis was further supported by the MWCO results of all TFC membranes as shown in **Fig. S12** of the SI: Specifically, membrane P1.5N0.5IP3 shows the lowest MWCO of 20000 Da, which represents the highest crosslinking degree and most dense structure. While membrane P1.5N0.5IP1 and P1.5N0.5IP5 have higher MWCO of 72000 Da and 35000 Da, respectively. As expected, the rejection for all model dyes exhibits a slight increase and then decrease, the trend of which is consistent with that of the membrane permeance. Although the theoretical molecular size of the

anionic dyes employed have MW lower than the MWCO of all four membranes presented in **Fig. 7c**, their dye rejection values are much higher than neutral PEG within the similar range of molecular weight (*e.g.*, 600-2000 Da). Therefore, the rejection behavior with anionic dyes of the as-prepared P[5]A-TFC membrane could be mainly attributed to the negatively charged nature of surface (**Section 3.4.2**). Based on the MWCO results, the P[5]A-TFC membranes could be tailored to fit for the isolation of neutral molecules of different sizes, for which further investigation is needed.

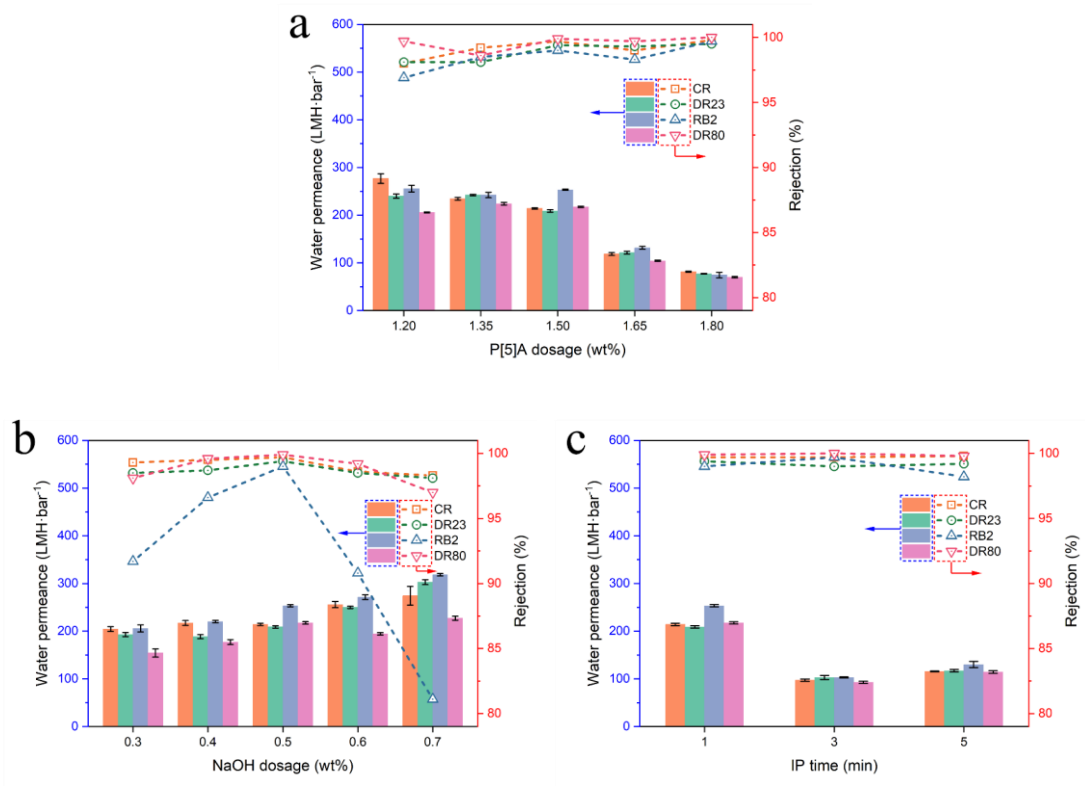

Fig. 7. Dye solution permeability and dye rejection rates of P[5]A-TFC membranes with (a) different P[5]A monomer dosages in aqueous solution; (b) different NaOH dosages in aqueous solution; and (c) different IP reaction times. (Each simulated feed contains a single dye, either CR, DR23, RB2 or DR80, of 200 ppm; applied pressure of cross-flow 2 bar; benchmarking synthesis conditions were P[5]A of 1.5 wt%, NaOH of 0.5 wt%, and IP time of 1 min).

Due to the simultaneous and competing effect of esterification and hydrolysis

during the studied IP reaction, careful choices of the membrane fabrication conditions should be made to ensure high solute rejection utilizing the dense cross-linked structure and reasonably high permeance utilizing the hydrolyzed loose structure of the IP layer. Based on the comparisons of synthesized P[5]A-TFC membranes, membrane P1.5N0.5IP1 demonstrated the most optimal performance in obtaining simultaneously high dye/salt selectivity and water permeability. Thus, P1.5N0.5IP1 was selected in the following filtration experiments with simulated dye/salt mixed solutions, exploring the long-term stability and membrane anti-fouling performance.

3.4.4. Effect of salinity on dye/salt fractionation performance

To verify the capability of the P[5]A-TFC membrane in the fractionation of dye and salt ions, **Fig. 8a** presents the filtration results with the optimal membrane P1.5N0.5IP1, using dye/salt mixed solutions containing a fixed concentration of DR23 (200 ppm) at varying Na_2SO_4 concentration from 0 to 40 g/L. It was shown that with the increasing content of Na_2SO_4, the rejection of dye remains constant in between 98.3% and 98.7%, demonstrating that membrane P1.5N0.5IP1 can stably decolorize regardless of the increasing salinity of the feed. This observation is encouraging but contrary to the adverse effect of increased feed salinity in the operation of conventional NF, which was reported to decrease the rejection of organic solutes possibly due to 1) the property change of the membranes (*e.g.*, increased pore size and/or thickness of the membrane) [82] and 2) shielding of the electrostatic interaction between surface and organic solutes [83]. Therefore, the extraordinary stability demonstrated by P1.5N0.5IP1 indicated that the robust cross-linking structure and angstrom-scale P[5]A channels can resist the widely-reported adverse salting effects and maintain high dye rejection in the tested range of salinity. However, the permeance decreases dramatically from 167.1 $LMH \cdot bar^{-1}$ to 8.0 $LMH \cdot bar^{-1}$, together with gradually increased salt rejection from 18.9% to 34.9%. In pressure-driven processes, the permeance of the membrane is directly related to the cross-membrane pressure difference, *i.e.*, the applied pressure subtracts the

osmotic pressure. When the former is kept constant and osmotic pressure differences increase with increasing salt concentration, it is reasonable to expect a decrease in process driving force and hence a flux decline [84, 85]. The flux decline could also be attributed to the "salting-out" effect under high salinity, which directly resulting in severe dye aggregation and dye/salt precipitation [84, 85]. Therefore, the deposition of salting-out particles may cause fouling formation. Meanwhile, a high salt concentration can decrease electrostatic repulsion between the membrane and charged solutes due to charge screening, which might also lead to the formation of a fouling layer and eventually flux decline [86].

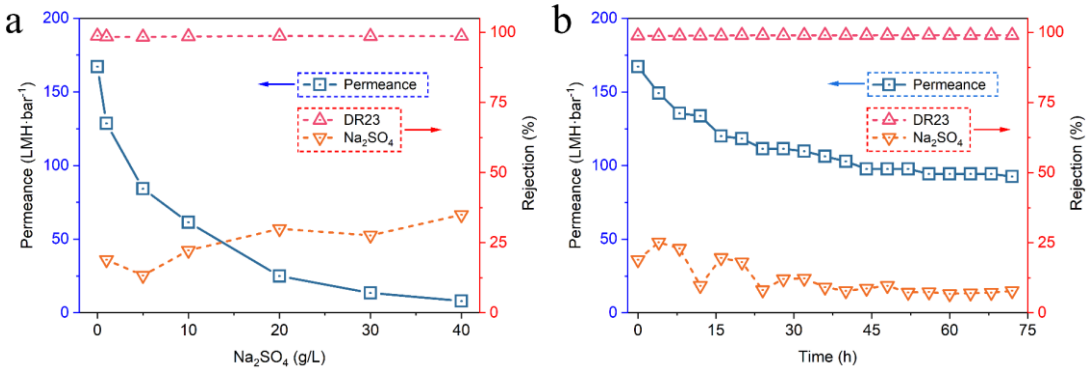

Fig. 8. Filtration performance of P1.5N0.5IP1 membrane (a) Effect of feed salinity; (b) semi long-term stability test (feed solution containing 200 ppm DR23 and 1 g/L Na_2SO_4; applied pressure at cross-flow 2 bar)

3.4.5. Stability of P[5]A-TFC membrane in dye/salt fractionation

Continuous experiments of 72 hours were performed to investigate the stability of P[5]A-TFC membrane for the fractionation of dye/salt mixture at constant solute concentration. The results are presented in **Fig. 8b** in terms of the permanence and solute rejection. During the first 24 h of operation, the water permeance decreases sharply from 167.1 to 111.4 LMH·bar^{-1}, equivalent to a decline of 33.3%; while from 24 to 48 h, the decreasing tendency becomes less significant, and eventually it stays around 92-94 LMH·bar^{-1} after 48 h. At the same time, the membrane demonstrates extremely stable dye rejection around 99.0% for DR23 ions. Slight fluctuations were observed in the Na_2SO_4 rejection, which gradually dropped and stabilized at around

7.2 % compared to the initial value of 18.9%. This could be explained with the membrane swelling and charge screening caused by salts, as well as the effective pore size increasing caused by "salting-out" effect [82, 87]. However, at a relatively lower range of salinity (1 g/L Na_2SO_4), the dye aggregation and dye/salt precipitation are minor. Therefore, the membrane fouling was mainly caused by the adsorption of dye molecules, which explains the slow decline of permeance [86].

Even after 72 h operating, the stabilized flux was nevertheless still as high as 92.6 LMH·bar^{-1} with overall stable solute rejection. As compared to the literature data summarized in **Section 3.4.7**, the permeance value obtained with the P[5]A-TFC membrane is still higher than most of the published data measured under short term experiments. Thus, the tested membrane has extraordinary stability and selectivity in continuous dye/salt fractionation. However, the gradual decline of permeance in the initial phase of the semi long-term operation is worth further investigation.

3.4.6. Anti-fouling performance of P[5]A-TFC membranes

Although membrane processes demonstrate very promising separation performances and possess a lot of advantages compared to other conventional technologies, membrane fouling has always been the major hindrance towards industrial scale applications [88]. Membrane fouling and scaling can directly result in flux decline, which can further lead to membrane productivity and economic losses. Besides, frequent cleaning would be required for recovering the membrane performance, which might cause membrane degradation and aging, shortening the membrane service life [21]. According to Chon et al., membrane fouling properties are closely related to surface charge and hydrophilicity characteristics [89]. Therefore, to evaluate the antifouling performance of the P[5]A-TFC membranes, a 2-cycle filtration experiment was done with intermediate pure water tests to benchmark the intactness of the membrane. The results are presented in **Fig. 9a** in terms of the normalized permeance as a function of the operating time, with single component solution

containing either DR23, RB2 or CR. In general, the membrane permeance declines whenever the feed is switched to a dye solution, by about 5 - 20% depending on the species of the dye, as compared to the pure water permeance. This phenomenon can be explained as the increased osmotic pressure due to the addition of dye solutes and concentration polarization adjacent to the membrane surface. The permeance decline when switching to the RB2 dye is least significant (5 - 10%); while those of CR and DR23 are both more (10 – 20%). This proves that the higher aggregation degree of direct dyes (*e.g.*, CR and DR23) can result in a larger effective size of solute during filtration, eventually leading to a more severe membrane fouling as discussed in **Section 3.4.3**.

The subsequent water permeance after the dye filtration in both the first and the second cycles shows that the rinsing procedure could repeatedly recover the membrane permeance to a great extent, regardless of the dye species. The ability of fouling resistance in each test scenario is expressed in terms of the fouling indices, *i.e.*, *FRR*, R_t, R_r, R_{ir}, calculated based on the permeance changes using Equations S4 – S7, the results shown in **Fig. 9b**. The *FRR* values for all three dye foulants are higher than 94%, which indicates that membrane P1.5N0.5IP1 has promising anti-fouling properties. As predicted, the R_{ir} values for all model foulants are lower than 6%, which indicates that the irreversible fouling caused by the deposition of dye aggregates could be greatly mitigated and hence minimal adsorption of dyes was observed. In general, the P[5]A-TFC membrane exhibited superior anti-fouling properties, which might be due to two reasons: firstly, the improved hydrophilicity (**Fig. 5a**) after IP modification imparts a hydration layer adjacent to the membrane surface, which can reduce foulant deposition; secondly, the electrostatic repulsion between the negative membrane surface (**Fig. 5b**) and the anionic dye ions; these two effects work synergistically to mitigate fouling formation. However, in the case of cationic dyes, *e.g.*, MB, strong adsorption of MB was observed (**Fig. S15b**) due to electrostatic attraction with negatively-charged surface and such surface contamination could not be easily removed by washing with DI water. This phenomena is in contrast with the minimal influence on the membrane used in

anionic dye filtration (**Fig. S15c**). Therefore, either further functionalization of the monomers to tailor the surface charge property or more efficient cleaning strategies (*e.g.*, with ethanol) should be explored in future studies to overcome the surface charge issue of the TFC membrane and broaden its applications in molecule fractionation and water / wastewater treatment in general.

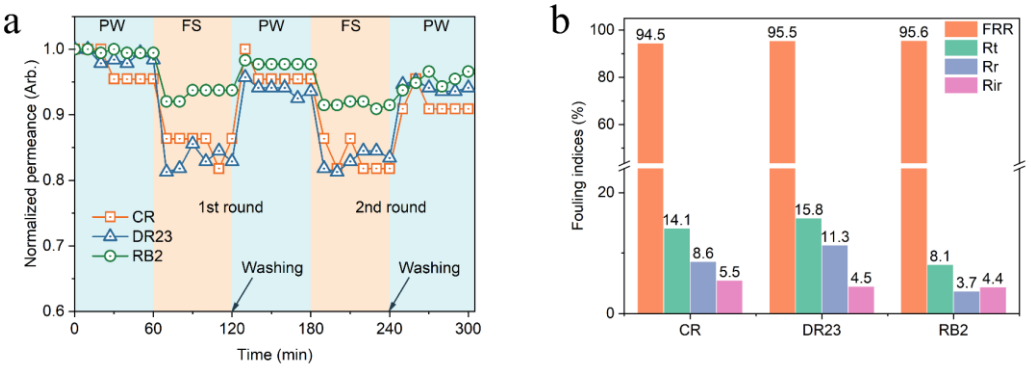

Fig. 9. Performance of membrane P1.5N0.5IP1 in 2-cycle fouling experiments (a) Normalized permeance in alternating pure water and dye solution testing; (b) flux recovery rate and fouling indices. (simulated feed solution: respective model dye of CR, DR23 or RB2 of 200 ppm, applied pressure of 2 bar)

3.4.7. Benchmarking membrane performance

To benchmark the performance of the as-developed P[5]A-TFC membrane in dye/salt fractionation, comparisons with similar membranes reported in recent literature are summarized in **Table S3** and **Fig. 10**, respectively. To better compare the membrane performance, all selected membranes were reported within the last 3 years and evaluated in the application of dye/salt fractionation with similar solutes under similar concentration ranges, *i.e.*, salt concentration of 500 - 2000 ppm, dye concentration of 20 - 200 ppm [90-100]. It is noted that only several membranes were made by the IP method; while the others were made by other methods such as ion cross-linking, in-situ growth, phase inversion, self-assembly. Compared to other membranes in **Table S3**, the as-developed membrane P1.5N0.5IP1 in this study exhibited a 3 – 10 times higher water permeance (267.1 LMH·bar^{-1}), which pointed towards the positive contribution of the

P[5]A water channels to the significantly improved permeability. The literature reported membranes all exhibited satisfactory dye retention performance of over 93.0% and high permeance to salts, *i.e.*, NaCl and Na_2SO_4. The separation factor $\alpha_{NaCl/CR}$ calculated based on **Equation S3** was used to evaluate the fractionation efficiency, *i.e.*, selectivity between NaCl and CR, where a high value of is α desired. As revealed in **Table S3** and **Fig. 10**, the membrane P1.5N0.5IP1 demonstrated an improved selectivity for salts and dyes, *e.g.*, $\alpha_{NaCl/CR}$ = 318.3, proving that the membrane selectivity was not compromised despite the ultra-high permeability.

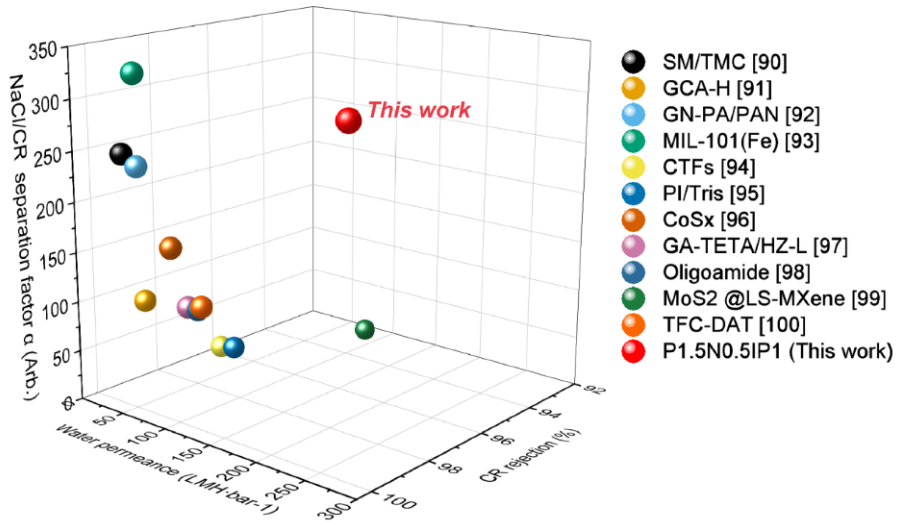

Fig. 10. Comparison of dye/salt filtration performance of advanced LNF membranes in literature during 2021-2023.

The extraordinary performance proves that P[5]A-TFC membranes have the potential to overcome the classical permeability/selectivity trade-off, achieving ultra-fast water treatment and precise molecular fractionation with a foreseeable prospect in energy saving and efficiency improvement.

4. Conclusions

In this study, a novel macrocycle P[5]A was selected as aqueous monomer to fabricate ultra-permeable dye/salt fractionation membranes with robust water channels *via* IP. Comprehensive characterizations prove that the as-developed P[5]A-TFC membranes possess enhanced hydrophilicity and negative surface charge due to the increased hydroxyl and carboxyl groups. The fabrication conditions including P[5]A concentration, NaOH dosage and IP time were investigated to control the competing effect of esterification and alkali-induced hydrolysis during IP layer formation. Consequently, an optimal membrane P1.5N0.5IP1 with ultra-high water permeance (267.1 LMH·bar^{-1}, 3 – 10 times higher than literature data) and precise dye/salt selectivity ($\alpha_{NaCl/CR}$ = 318.3) was developed. The superior performance pointed towards the water channel effect of the P[5]A intramolecular cavity, which can greatly enhance the membrane permeability without compromising the selectivity. This membrane also demonstrated stable performance in separating dye/salt mixtures under continuous experiment, and good capability in fractionating of dye/salt mixtures with high salinity. Attributed to the intrinsic angstrom-scale cavity of P[5]A, enhanced hydrophilicity and negative surface charge, this membrane was also endowed with excellent anti-fouling properties. Moreover, further exploration of functionalized macrocycles which tailor the membrane properties to broaden its applications is foreseeable. Overall, the membrane and method developed in this study possess prosperous application potential in ultra-fast waste source recovery and other precise products fractionation processes.

ASSOCIATED CONTENT

Supporting Information

Fig. S1. Per-methoxypillar[5]arene; **Fig. S2.** The ^{1}H-NMR spectrum of per-methoxypillar[5]arene; **Fig. S3.** The ^{13}C-NMR spectrum of per-methoxypillar[5]arene;

Fig. S4. Per-hydroxypillar[5]arene; **Fig. S5.** The ^{1}H-NMR spectrum of per-hydroxypillar[5]arene; **Fig. S6.** The ^{13}C-NMR spectrum of per-hydroxypillar[5]arene; **Fig. S7.** Schematic of lab-assembled scale cross-flow apparatus; **Fig. S8.** Chemical characterization of PES substrate and P[5]A-TFC membranes. (a) The C 1s spectra of P1.35N0.5IP1; (b) The C 1s spectra of P1.65N0.5IP1; (c) The C 1s spectra of P1.5N0.4IP1; (d) The C 1s spectra of P1.5N0.6IP1; (e) The C 1s spectra of P1.5N0.5IP3; (f) The C 1s spectra of P1.5N0.5IP5; **Fig. S9.** (a) The surface morphology of PES substrate, (SEM image); (b) the AFM image and the root-mean-square roughness (RMS) of PES substrate; (c) cross-sectional morphology of PES substrate, (SEM image).; **Fig. S10.** The surface morphology of P[5]A-TFC membranes by varying P[5]A monomer concentration (a) P1.35N0.5IP1, (b)P1.5N0.5IP1, (c)P1.65N0.5IP1, (SEM image); the AFM images and the root-mean-square roughness (RMS) of (d) P1.35N0.5IP1, (e)P1.5N0.5IP1, (f)P1.65N0.5IP1; cross-sectional morphology of (g) P1.35N0.5IP1, (h)P1.5N0.5IP1, (i)P1.65N0.5IP1, (SEM image); **Fig. S11.** The surface morphology of P[5]A-TFC membranes by varying NaOH concentration (a) P1.5N0.4IP1, (b)P1.5N0.5IP1, (c)P1.5N0.6IP1, (SEM image); the AFM images and the root-mean-square roughness (RMS) of (d) P1.5N0.4IP1, (e)P1.5N0.5IP1, (f)P1.5N0.6IP1; cross-sectional morphology of (g) P1.5N0.4IP1, (h) P1.5N0.5IP1, (i) P1.5N0.6IP1, (SEM image). **Fig. S12.** The MWCO of PES substrate and P1.5N0.5IP1, P1.5N0.5IP3, P1.5N0.5IP5 membranes. **Fig. S13.** Permeance, salt rejection and dye rejection of PES15 substrate (applied pressure in cross-flow: 2 bar; salt concentration: 1000 ppm; dye concentration: 200 ppm). **Fig. S14.** Permeance and dye rejection of membrane P1.5N0.5IP1 (applied pressure in cross-flow: 2 bar; dye concentration: 200 ppm). **Fig. S15.** Picture of P1.5N0.5IP1 membrane (a) fresh membrane; (b) after MB testing; (c) after CR testing. **Table S1** The chemical structures of selected dye ions; **Table S2** Elemental composition of PES substrate and P[5]A-TFC membranes as determined from XPS survey spectra. **Table S3**. Comparison of dye/salt filtration performance of advanced membranes in literature (2021-2023).

Declaration of Competing Interest

The authors declare that they have no known competing financial interests or personal relationships that could have appeared to influence the work reported in this paper.

ACKNOWLEDGEMENTS

The authors would like to acknowledge the support provided by China Scholarship Council (CSC) of the Ministry of Education, P.R.China (CSC No. 202107650055) (J. H), Research Foundation – Flanders (FWO) Odysseus grant (G0F7621N) (X.Y & J.H), the FWO fundamental research project 11G8121N (S.B), the KU Leuven project STG/20/023 ((X.Y) and C14/18/061 (S.E & W.T). The authors thank the experimental and technical help from Dr. Laurens Rutgeerts from the Department of Microbial and Molecular Systems, Mrs. Christine Wouters and Mr. Herman Tollet from the Department of Chemical Engineering at KU Leuven.

REFERENCES

[1] T.A. Saleh, V.K. Gupta, An Overview of Membrane Science and Technology, in: T.A. Saleh, V.K. Gupta (Eds.), Nanomaterial and Polymer Membranes, Elsevier2016, pp. 1-23. https://doi.org/10.1016/b978-0-12-804703-3.00001-2.

[2] A.G. Fane, R. Wang, Y. Jia, Membrane Technology: Past, Present and Future, in: L.K. Wang, J.P. Chen, Y.-T. Hung, N.K. Shammas (Eds.), Membrane and Desalination Technologies, Humana Press, Totowa, NJ, 2011, pp. 1-45. https://doi.org/10.1007/978-1-59745-278-6_1.

[3] C. Klaysom, T.Y. Cath, T. Depuydt, I.F. Vankelecom, Forward and pressure retarded osmosis: potential solutions for global challenges in energy and water supply,

781 Chem Soc Rev 42(16) (2013) 6959-89. https://doi.org/10.1039/c3cs60051c.
782 [4] Q. Zhao, Q.F.F. An, Y.L. Ji, J.W. Qian, C.J. Gao, Polyelectrolyte complex
783 membranes for pervaporation, nanofiltration and fuel cell applications, Journal of
784 Membrane Science 379(1-2) (2011) 19-45.
785 https://doi.org/10.1016/j.memsci.2011.06.016.
786 [5] E. Drioli, A.I. Stankiewicz, F. Macedonio, Membrane engineering in process
787 intensification—An overview, Journal of Membrane Science 380(1-2) (2011) 1-8.
788 https://doi.org/10.1016/j.memsci.2011.06.043.
789 [6] B. Van der Bruggen, L. Braeken, The challenge of zero discharge: from water
790 balance to regeneration, Desalination 188(1-3) (2006) 177-183.
791 https://doi.org/10.1016/j.desal.2005.04.115.
792 [7] R. Al-Tohamy, S.S. Ali, F. Li, K.M. Okasha, Y.A. Mahmoud, T. Elsamahy, H. Jiao,
793 Y. Fu, J. Sun, A critical review on the treatment of dye-containing wastewater:
794 Ecotoxicological and health concerns of textile dyes and possible remediation
795 approaches for environmental safety, Ecotoxicol Environ Saf 231 (2022) 113160.
796 https://doi.org/10.1016/j.ecoenv.2021.113160.
797 [8] L. Wang, N.X. Wang, G.J. Zhang, S.L. Ji, Covalent Crosslinked Assembly of
798 Tubular Ceramic-based Multilayer Nanofiltration Membranes for Dye Desalination,
799 Aiche Journal 59(10) (2013) 3834-3842. https://doi.org/10.1002/aic.14093.
800 [9] X.Z. Wei, X. Kong, C.T. Sun, J.Y. Chen, Characterization and application of a
801 thin-film composite nanofiltration hollow fiber membrane for dye desalination and
802 concentration, Chemical Engineering Journal 223 (2013) 172-182.
803 https://doi.org/10.1016/j.cej.2013.03.021.
804 [10] I. De Vreese, B. Van der Bruggen, Cotton and polyester dyeing using nanofiltered
805 wastewater, Dyes and Pigments 74(2) (2007) 313-319.
806 https://doi.org/10.1016/j.dyepig.2006.02.014.
807 [11] J.Y. Lin, W.Y. Ye, H.M. Zeng, H. Yang, J.N. Shen, S. Darvishmanesh, P. Luis, A.
808 Sotto, B. Van der Bruggen, Fractionation of direct dyes and salts in aqueous solution
809 using loose nanofiltration membranes, Journal of Membrane Science 477 (2015) 183-
810 193. https://doi.org/10.1016/j.memsci.2014.12.008.
811 [12] J. Huang, K.S. Zhang, The high flux poly (m-phenylene isophthalamide)
812 nanofiltration membrane for dye purification and desalination, Desalination 282
813 (2011) 19-26. https://doi.org/10.1016/j.desal.2011.09.045.
814 [13] Y. He, G.M. Li, H. Wang, J.F. Zhao, H.X. Su, Q.Y. Huang, Effect of operating
815 conditions on separation performance of reactive dye solution with membrane
816 process, Journal of Membrane Science 321(2) (2008) 183-189.
817 https://doi.org/10.1016/j.memsci.2008.04.056.
818 [14] A.C. Jadhav, N.C. Jadhav, Treatment of textile wastewater using adsorption and

adsorbents, in: S.S. Muthu (Ed.), Sustainable Technologies for Textile Wastewater Treatments, Woodhead Publishing2021, pp. 235-273. https://doi.org/10.1016/b978-0-323-85829-8.00008-0.
[15] A. Ahmad, S.H. Mohd-Setapar, C.S. Chuong, A. Khatoon, W.A. Wani, R. Kumar, M. Rafatullah, Recent advances in new generation dye removal technologies: novel search for approaches to reprocess wastewater, Rsc Advances 5(39) (2015) 30801-30818. https://doi.org/10.1039/c4ra16959j.
[16] M. Greluk, Z. Hubicki, Efficient removal of Acid Orange 7 dye from water using the strongly basic anion exchange resin Amberlite IRA-958, Desalination 278(1-3) (2011) 219-226. https://doi.org/10.1016/j.desal.2011.05.024.
[17] A.R. Rahmani, A. Mousavi-Tashar, Z. Masoumi, G. Azarian, Integrated advanced oxidation process, sono-Fenton treatment, for mineralization and volume reduction of activated sludge, Ecotoxicol Environ Saf 168 (2019) 120-126. https://doi.org/10.1016/j.ecoenv.2018.10.069.
[18] L. Liu, L. Yu, B. Borjigin, Q. Liu, C. Zhao, D. Hou, Fabrication of thin-film composite nanofiltration membranes with improved performance using β-cyclodextrin as monomer for efficient separation of dye/salt mixtures, Applied Surface Science 539 (2021) 148284. https://doi.org/10.1016/j.apsusc.2020.148284.
[19] Y.F. Li, Y.L. Su, X.T. Zhao, R.N. Zhang, J.J. Zhao, X.C. Fan, Z.Y. Jiang, Surface fluorination of polyamide nanofiltration membrane for enhanced antifouling property, Journal of Membrane Science 455 (2014) 15-23. https://doi.org/10.1016/j.memsci.2013.12.060.
[20] F. Yan, H. Chen, Y. Lu, Z.H. Lu, S.C. Yu, M.H. Liu, C.J. Gao, Improving the water permeability and antifouling property of thin-film composite polyamide nanofiltration membrane by modifying the active layer with triethanolamine, Journal of Membrane Science 513 (2016) 108-116. https://doi.org/10.1016/j.memsci.2016.04.049.
[21] A.W. Mohammad, Y.H. Teow, W.L. Ang, Y.T. Chung, D.L. Oatley-Radcliffe, N. Hilal, Nanofiltration membranes review: Recent advances and future prospects, Desalination 356 (2015) 226-254. https://doi.org/10.1016/j.desal.2014.10.043.
[22] I. Nulens, A. Ben Zvi, I.F.J. Vankelecom, G.Z. Ramon, Re-thinking polyamide thin film formation: How does interfacial destabilization dictate film morphology?, Journal of Membrane Science 656 (2022) 120593. https://doi.org/10.1016/j.memsci.2022.120593.
[23] M.B.M.Y. Ang, G.W. Huang, M.Y. Chu, J.C. Millare, S.H. Huang, K.R. Lee, Use of aqueous polyol monomer for superior dye separation performance and high chlorine resistance of thin-film composite polyester nanofiltration membranes, Journal of Water Process Engineering 48 (2022) 102843.

https://doi.org/10.1016/j.jwpe.2022.102843.
[24] M.R. Chowdhury, J. Steffes, B.D. Huey, J.R. McCutcheon, 3D printed polyamide membranes for desalination, Science (New York, N.Y.) 361(6403) (2018) 682-686. https://doi.org/10.1126/science.aar2122.
[25] W.J. Lau, A.F. Ismail, N. Misdan, M.A. Kassim, A recent progress in thin film composite membrane: A review, Desalination 287 (2012) 190-199. https://doi.org/10.1016/j.desal.2011.04.004.
[26] G. Gong, P. Wang, Z. Zhou, Y. Hu, New Insights into the Role of an Interlayer for the Fabrication of Highly Selective and Permeable Thin-Film Composite Nanofiltration Membrane, ACS Appl Mater Interfaces 11(7) (2019) 7349-7356. https://doi.org/10.1021/acsami.8b18719.
[27] M.N.A. Seman, M. Khayet, N. Hilal, Nanofiltration thin-film composite polyester polyethersulfone-based membranes prepared by interfacial polymerization, Journal of Membrane Science 348(1-2) (2010) 109-116. https://doi.org/10.1016/j.memsci.2009.10.047.
[28] S.S. Yuan, G. Zhang, J.F. Zheng, P.R. Jin, J.Y. Zhu, J. Yang, S.L. Liu, P. Van Puyvelde, B. Van der Bruggen, Tuning intermolecular pores of resorcin[4]arene-based membranes for enhanced nanofiltration performance, Journal of Membrane Science 610 (2020) 118282. https://doi.org/10.1016/j.memsci.2020.118282.
[29] X. He, H. Sin, B. Liang, Z.A. Ghazi, A.M. Khattak, N.A. Khan, H.R. Alanagh, L.S. Li, X.Q. Lu, Z.Y. Tang, Controlling the Selectivity of Conjugated Microporous Polymer Membrane for Efficient Organic Solvent Nanofiltration, Advanced Functional Materials 29(32) (2019) 1900134. https://doi.org/10.1002/adfm.201900134.
[30] M. Di Vincenzo, A. Tiraferri, V.E. Musteata, S. Chisca, M. Deleanu, F. Ricceri, D. Cot, S.P. Nunes, M. Barboiu, Tunable membranes incorporating artificial water channels for high-performance brackish/low-salinity water reverse osmosis desalination, Proc Natl Acad Sci U S A 118(37) (2021) e2022200118. https://doi.org/10.1073/pnas.2022200118.
[31] D. Strilets, S. Cerneaux, M. Barboiu, Enhanced Desalination Polyamide Membranes Incorporating Pillar[5]arene through in-Situ Aggregation-Interfacial Polymerization-isAGRIP, Chempluschem 86(12) (2021) 1602-1607. https://doi.org/10.1002/cplu.202100473.
[32] J. Cai, X.-L. Cao, Y. Zhao, F.-Y. Zhou, Z. Cui, Y. Wang, S.-P. Sun, The establishment of high-performance anti-fouling nanofiltration membranes via cooperation of annular supramolecular Cucurbit[6]uril and dendritic polyamidoamine, Journal of Membrane Science 600 (2020). https://doi.org/10.1016/j.memsci.2020.117863.

[33] X.L. Cao, J.L. Guo, J. Cai, M.L. Liu, S. Japip, W. Xing, S.P. Sun, The encouraging improvement of polyamide nanofiltration membrane by cucurbituril-based host–guest chemistry, AIChE Journal 66(4) (2019) e16879. https://doi.org/10.1002/aic.16879.
[34] L.F. Villalobos, T. Huang, K.V. Peinemann, Cyclodextrin Films with Fast Solvent Transport and Shape-Selective Permeability, Adv Mater 29(26) (2017) 1606641. https://doi.org/10.1002/adma.201606641.
[35] Z. Zhai, C. Jiang, N. Zhao, W.J. Dong, P. Li, H.X. Sun, Q.J. Niu, Polyarylate membrane constructed from porous organic cage for high-performance organic solvent nanofiltration, Journal of Membrane Science 595 (2020) 117505. https://doi.org/10.1016/j.memsci.2019.117505.
[36] L.L. Zhao, X.L. Cao, C. Luo, Q. Wang, T.D. Lu, M.J. Tang, S.P. Sun, W. Xing, Locking Patterned Carbon Nanotube Cages by Nanofibrous Mats to Construct Cucurbituril[n]-Based Ultrapermselective Dye/Salt Separation Membranes, Nano Lett 23(10) (2023) 4167-4175. https://doi.org/10.1021/acs.nanolett.2c05105.
[37] T. Ogoshi, S. Kanai, S. Fujinami, T.A. Yamagishi, Y. Nakamoto, para-Bridged symmetrical pillar[5]arenes: their Lewis acid catalyzed synthesis and host-guest property, J Am Chem Soc 130(15) (2008) 5022-3. https://doi.org/10.1021/ja711260m.
[38] D. Cao, Y. Kou, J. Liang, Z. Chen, L. Wang, H. Meier, A facile and efficient preparation of pillararenes and a pillarquinone, Angew Chem Int Ed Engl 48(51) (2009) 9721-3. https://doi.org/10.1002/anie.200904765.
[39] T. Ogoshi, T.A. Yamagishi, Y. Nakamoto, Pillar-Shaped Macrocyclic Hosts Pillar[n]arenes: New Key Players for Supramolecular Chemistry, Chem Rev 116(14) (2016) 7937-8002. https://doi.org/10.1021/acs.chemrev.5b00765.
[40] Y.Y. Fang, Y. Deng, W. Dehaen, Tailoring pillararene-based receptors for specific metal ion binding: From recognition to supramolecular assembly, Coordination Chemistry Reviews 415 (2020). https://doi.org/10.1016/j.ccr.2020.213313.
[41] M. Xue, Y. Yang, X. Chi, Z. Zhang, F. Huang, Pillararenes, a new class of macrocycles for supramolecular chemistry, Acc Chem Res 45(8) (2012) 1294-308. https://doi.org/10.1021/ar2003418.
[42] W.X. Feng, Z.H. Sun, M. Barboiu, Pillar[n]arenes for Construction of Artificial Transmembrane Channels, Isr J Chem 58(11) (2018) 1173-1182. https://doi.org/10.1002/ijch.201800017.
[43] N. Song, T. Kakuta, T.A. Yamagishi, Y.W. Yang, T. Ogoshi, Molecular-Scale Porous Materials Based on Pillar[n]arenes, Chem 4(9) (2018) 2029-2053. https://doi.org/10.1016/j.chempr.2018.05.015.
[44] Y.X. Shen, W. Song, D.R. Barden, T. Ren, C. Lang, H. Feroz, C.B. Henderson, P.O. Saboe, D. Tsai, H. Yan, P.J. Butler, G.C. Bazan, W.A. Phillip, R.J. Hickey, P.S.

933 Cremer, H. Vashisth, M. Kumar, Achieving high permeability and enhanced
934 selectivity for Angstrom-scale separations using artificial water channel membranes,
935 Nat Commun 9(1) (2018) 2294. https://doi.org/10.1038/s41467-018-04604-y.
936 [45] X.B. Hu, Z. Chen, G. Tang, J.L. Hou, Z.T. Li, Single-molecular artificial
937 transmembrane water channels, J Am Chem Soc 134(20) (2012) 8384-7.
938 https://doi.org/10.1021/ja302292c.
939 [46] W. Si, L. Chen, X.B. Hu, G. Tang, Z. Chen, J.L. Hou, Z.T. Li, Selective artificial
940 transmembrane channels for protons by formation of water wires, Angew Chem Int
941 Ed Engl 50(52) (2011) 12564-8. https://doi.org/10.1002/anie.201106857.
942 [47] Q. Zhao, Y. Liu, Macrocycle crosslinked mesoporous polymers for ultrafast
943 separation of organic dyes, Chem Commun (Camb) 54(53) (2018) 7362-7365.
944 https://doi.org/10.1039/c8cc04080j.
945 [48] W.M. Fu, Y.Z. Huang, L.Y. Deng, J.H. Sun, S.L. Li, Y.X. Hu, Ultra-thin
946 microporous membranes based on macrocyclic pillar[n]arene for efficient organic
947 solvent nanofiltration, Journal of Membrane Science 655 (2022) 120583.
948 https://doi.org/10.1016/j.memsci.2022.120583.
949 [49] P. Arribas, M.C. Garcia-Payo, M. Khayet, L. Gil, Improved antifouling
950 performance of polyester thin film nanofiber composite membranes prepared by
951 interfacial polymerization, Journal of Membrane Science 598 (2020) 117774.
952 https://doi.org/10.1016/j.memsci.2019.117774.
953 [50] L. Ma, S. Wang, C. Li, D. Cao, T. Li, X. Ma, Photo-controlled fluorescence
954 on/off switching of a pseudo[3]rotaxane between an AIE-active pillar[5]arene host
955 and a photochromic bithienylethene guest, Chem Commun (Camb) 54(19) (2018)
956 2405-2408. https://doi.org/10.1039/c8cc00213d.
957 [51] T. Ogoshi, K. Kitajima, T.A. Yamagishi, Y. Nakamoto, Synthesis and
958 conformational characteristics of nonsymmetric pillar[5]arene, Org Lett 12(3) (2010)
959 636-8. https://doi.org/10.1021/ol902877w.
960 [52] S. Pan, J. Li, O. Noonan, X. Fang, G. Wan, C. Yu, L. Wang, Dual-Functional
961 Ultrafiltration Membrane for Simultaneous Removal of Multiple Pollutants with High
962 Performance, Environ Sci Technol 51(9) (2017) 5098-5107.
963 https://doi.org/10.1021/acs.est.6b05295.
964 [53] A.K. Hołda, I.F.J. Vankelecom, Understanding and guiding the phase inversion
965 process for synthesis of solvent resistant nanofiltration membranes, Journal of
966 Applied Polymer Science 132(27) (2015) n/a-n/a. https://doi.org/10.1002/app.42130.
967 [54] L. Wang, N.X. Wang, J. Li, J.W. Li, W.W. Bian, S.L. Ji, Layer-by-layer self-
968 assembly of polycation/GO nanofiltration membrane with enhanced stability and
969 fouling resistance, Separation and Purification Technology 160 (2016) 123-131.
970 https://doi.org/10.1016/j.seppur.2016.01.024.

[55] A. Asatekin, S. Kang, M. Elimelech, A.M. Mayes, Anti-fouling ultrafiltration membranes containing polyacrylonitrile-graft-poly (ethylene oxide) comb copolymer additives, Journal of Membrane Science 298(1-2) (2007) 136-146. https://doi.org/10.1016/j.memsci.2007.04.011.
[56] Y.Z. Liang, X.X. Teng, R. Chen, Y.Z. Zhu, J. Jin, S.H. Lin, Polyamide Nanofiltration Membranes from Emulsion-Mediated Interfacial Polymerization, Acs Es&T Engineering 1(3) (2021) 533-542. https://doi.org/10.1021/acsestengg.0c00213.
[57] J. Liu, D. Hua, Y. Zhang, S. Japip, T.S. Chung, Precise Molecular Sieving Architectures with Janus Pathways for Both Polar and Nonpolar Molecules, Adv Mater 30(11) (2018) 1705933. https://doi.org/10.1002/adma.201705933.
[58] N. Evenepoel, S. Wen, M. Tilahun Tsehaye, B. Van der Bruggen, Potential of DMSO as greener solvent for PES ultra- and nanofiltration membrane preparation, 135(28) (2018) 46494. https://doi.org/10.1002/app.46494.
[59] Z. Tan, S. Chen, X. Peng, L. Zhang, C. Gao, Polyamide membranes with nanoscale Turing structures for water purification, Science (New York, N.Y.) 360(6388) (2018) 518-521. https://doi.org/10.1126/science.aar6308.
[60] Y.J. Song, P. Sun, L.L. Henry, B.H. Sun, Mechanisms of structure and performance controlled thin film composite membrane formation via interfacial polymerization process, Journal of Membrane Science 251(1-2) (2005) 67-79. https://doi.org/10.1016/j.memsci.2004.10.042.
[61] J.S. Trivedi, D.V. Bhalani, G.R. Bhadu, S.K. Jewrajka, Multifunctional amines enable the formation of polyamide nanofilm composite ultrafiltration and nanofiltration membranes with modulated charge and performance, Journal of Materials Chemistry A 6(41) (2018) 20242-20253. https://doi.org/10.1039/c8ta07841f.
[62] P.R. Jin, J.Y. Zhu, S.S. Yuan, G. Zhang, A. Volodine, M.M. Tian, J.X. Wang, P. Luis, B. Van der Bruggen, Erythritol-based polyester loose nanofiltration membrane with fast water transport for efficient dye/salt separation, Chemical Engineering Journal 406 (2021) 126796. https://doi.org/10.1016/j.cej.2020.126796.
[63] J.Y. Zhu, S.S. Yuan, A. Uliana, J.W. Hou, J. Li, X. Li, M.M. Tian, Y. Chen, A. Volodin, B. Van der Bruggen, High-flux thin film composite membranes for nanofiltration mediated by a rapid co-deposition of polydopamine/piperazine, Journal of Membrane Science 554 (2018) 97-108. https://doi.org/10.1016/j.memsci.2018.03.004.
[64] R.H. Ma, X.L. Lu, S.Z. Zhang, K. Ren, J. Gu, C. Liu, Z.Q. Liu, H.L. Wang, Constructing discontinuous silicon-island structure with low surface energy based on the responsiveness of hydrophilic layers to improve the anti-fouling property of membranes, Journal of Membrane Science 659 (2022) 120770.

https://doi.org/10.1016/j.memsci.2022.120770.
[65] N.H. Ismail, W.N.W. Salleh, A.F. Ismail, H. Hasbullah, N. Yusof, F. Aziz, J. Jaafar, Hydrophilic polymer-based membrane for oily wastewater treatment: A review, Separation and Purification Technology 233 (2020) 116007. https://doi.org/10.1016/j.seppur.2019.116007.
[66] S.L. Huang, R.H.A. Ras, X.L. Tian, Antifouling membranes for oily wastewater treatment: Interplay between wetting and membrane fouling, Current Opinion in Colloid & Interface Science 36 (2018) 90-109. https://doi.org/10.1016/j.cocis.2018.02.002.
[67] S. Xiang, X.X. Tang, S. Rajabzadeh, P.F. Zhang, Z.Y. Cui, H. Matsuyama, Fabrication of PVDF/EVOH blend hollow fiber membranes with hydrophilic property via thermally induced phase process, Separation and Purification Technology 301 (2022) 122031. https://doi.org/10.1016/j.seppur.2022.122031.
[68] A.W. Qin, X.L. Wu, B.M. Ma, X.Z. Zhao, C.J. He, Enhancing the antifouling property of poly(vinylidene fluoride)/SiO2 hybrid membrane through TIPS method, Journal of Materials Science 49(22) (2014) 7797-7808. https://doi.org/10.1007/s10853-014-8490-y.
[69] Y.Q. Zhang, X.Q. Cheng, X. Jiang, J.J. Urban, C.H. Lau, S.Q. Liu, L. Shao, Robust natural nanocomposites realizing unprecedented ultrafast precise molecular separations, Materials Today 36 (2020) 40-47. https://doi.org/10.1016/j.mattod.2020.02.002.
[70] B.B. Tang, Z.B. Huo, P.Y. Wu, Study on a novel polyester composite nanofiltration membrane by interfacial polymerization of triethanolamine (TEOA) and trimesoyl chloride (TMC) I. Preparation, characterization and nanofiltration properties test of membrane, Journal of Membrane Science 320(1-2) (2008) 198-205. https://doi.org/10.1016/j.memsci.2008.04.002.
[71] C. Gleissner, J. Landsiedel, T. Bechtold, T. Pham, Surface Activation of High Performance Polymer Fibers: A Review, Polymer Reviews 62(4) (2022) 757-788. https://doi.org/10.1080/15583724.2022.2025601.
[72] M.S. Han, Y. Park, C.H. Park, Development of Superhydrophobic Polyester Fabrics Using Alkaline Hydrolysis and Coating with Fluorinated Polymers, Fibers and Polymers 17(2) (2016) 241-247. https://doi.org/10.1007/s12221-016-5693-7.
[73] H. Tavanai, A new look at the modification of polyethylene terephthalate by sodium hydroxide, Journal of the Textile Institute 100(7) (2009) 633-639. https://doi.org/10.1080/00405000802128489.
[74] Z.Y. Wang, S.M. Liang, Y. Kang, W. Zhao, Y. Xia, J.D. Yang, H.T. Wang, X.W. Zhang, Manipulating interfacial polymerization for polymeric nanofilms of composite separation membranes, Progress in Polymer Science 122 (2021) 101450.

https://doi.org/10.1016/j.progpolymsci.2021.101450.
[75] J.W. Zhang, S.Y. Huang, H. Guo, A.G. Fane, C.Y. Tang, Effects of crossflow filtration cell configuration on membrane separation performance and fouling behaviour, Desalination 525 (2022) 115505. https://doi.org/10.1016/j.desal.2021.115505.
[76] D. Vezzani, S. Bandini, Donnan equilibrium and dielectric exclusion for characterization of nanofiltration membranes, Desalination 149(1-3) (2002) 477-483. https://doi.org/10.1016/S0011-9164(02)00784-1.
[77] D. Yadav, S. Karki, P.G. Ingole, Current advances and opportunities in the development of nanofiltration (NF) membranes in the area of wastewater treatment, water desalination, biotechnological and pharmaceutical applications, Journal of Environmental Chemical Engineering 10(4) (2022) 108109. https://doi.org/10.1016/j.jece.2022.108109.
[78] J. Schaep, B. Van der Bruggen, C. Vandecasteele, D. Wilms, Influence of ion size and charge in nanofiltration, Separation and Purification Technology 14(1-3) (1998) 155-162. https://doi.org/10.1016/S1383-5866(98)00070-7.
[79] J.Y. Lin, W.Y. Ye, M.C. Baltaru, Y.P. Tang, N.J. Bernstein, P. Gao, S. Balta, M. Vlad, A. Volodin, A. Sotto, P. Luis, A.L. Zydney, B. Van der Bruggen, Tight ultrafiltration membranes for enhanced separation of dyes and Na2SO4 during textile wastewater treatment, Journal of Membrane Science 514 (2016) 217-228. https://doi.org/10.1016/j.memsci.2016.04.057.
[80] K. Hamada, H. Nonogaki, Y. Fukushima, B. Munkhbat, M. Mitsuishi, Effects of Hydrating Water-Molecules on the Aggregation Behavior of Azo Dyes in Aqueous-Solutions, Dyes and Pigments 16(2) (1991) 111-118. https://doi.org/10.1016/0143-7208(91)85003-Q.
[81] M. Jiang, K. Ye, J. Deng, J. Lin, W. Ye, S. Zhao, B. Van der Bruggen, Conventional Ultrafiltration As Effective Strategy for Dye/Salt Fractionation in Textile Wastewater Treatment, Environ Sci Technol 52(18) (2018) 10698-10708. https://doi.org/10.1021/acs.est.8b02984.
[82] J.Q. Luo, Y.H. Wan, Effect of highly concentrated salt on retention of organic solutes by nanofiltration polymeric membranes, Journal of Membrane Science 372(1-2) (2011) 145-153. https://doi.org/10.1016/j.memsci.2011.01.066.
[83] V. Freger, T.C. Arnot, J.A. Howell, Separation of concentrated organic/inorganic salt mixtures by nanofiltration, Journal of Membrane Science 178(1-2) (2000) 185-193. https://doi.org/10.1016/S0376-7388(00)00516-0.
[84] R. Jiraratananon, A. Sungpet, P. Luangsowan, Performance evaluation of nanofiltration membranes for treatment of effluents containing reactive dye and salt, Desalination 130(2) (2000) 177-183. https://doi.org/10.1016/S0011-9164(00)00085-0.

[85] I. Koyuncu, D. Topacik, M.R. Wiesner, Factors influencing flux decline during nanofiltration of solutions containing dyes and salts, Water Res 38(2) (2004) 432-40. https://doi.org/10.1016/j.watres.2003.10.001.
[86] G. Egabaierdi, H.B. Yu, Y. Li, X.Q. Zhang, H.O. Song, M.X. Du, Effect of dye aggregation and salting-out on membrane fouling and control measures during nanofiltration of saline dye wastewater, Journal of Water Process Engineering 50 (2022) 103285. https://doi.org/10.1016/j.jwpe.2022.103285.
[87] M. Nilsson, G. Tragardh, K. Ostergren, The influence of pH, salt and temperature on nanofiltration performance, Journal of Membrane Science 312(1-2) (2008) 97-106. https://doi.org/10.1016/j.memsci.2007.12.059.
[88] C.Y. Tang, T.H. Chong, A.G. Fane, Colloidal interactions and fouling of NF and RO membranes: a review, Adv Colloid Interface Sci 164(1-2) (2011) 126-43. https://doi.org/10.1016/j.cis.2010.10.007.
[89] K. Chon, J. Cho, H.K. Shon, Fouling characteristics of a membrane bioreactor and nanofiltration hybrid system for municipal wastewater reclamation, Bioresour Technol 130 (2013) 239-47. https://doi.org/10.1016/j.biortech.2012.12.007.
[90] Y.Y. Liu, J. Du, H.W. Wu, C. Cong, H.F. Zhang, J.X. Wang, Z. Wang, Antifouling streptomycin-based nanofiltration membrane with high permselectivity for dye/salt separation, Separation and Purification Technology 297 (2022) 121443. https://doi.org/10.1016/j.seppur.2022.121443.
[91] K.Y. Zhao, M. Chen, Y. Zhang, J.P. Miao, J. Jiang, W.B. Xie, Z.H. Yang, L.G. Lin, W. Zhang, R.R. Chu, W.X. Shi, Y.X. Hu, Anti-fouling and anti-bacterial graphene oxide/calcium alginate hybrid hydrogel membrane for efficient dye/salt separation, Desalination 538 (2022) 115908. https://doi.org/10.1016/j.desal.2022.115908.
[92] H. Zhang, T. Zhang, S. Ding, X. Wang, Development of loose thin film nanofibrous composite nanofiltration membrane with modified g-C3N4 nanosheets barrier layer for efficient separation of salt/dye mixtures, Separation and Purification Technology 306 (2023) 122661. https://doi.org/10.1016/j.seppur.2022.122661.
[93] Y.H. Tong, Y.Z. Wu, Z.L. Xu, L.H. Luo, S.J. Xu, Photocatalytic self-cleaning EVAL membrane by incorporating bio-inspired functionalized MIL-101(Fe) for dye/salt separation, Chemical Engineering Journal 444 (2022) 136507. https://doi.org/10.1016/j.cej.2022.136507.
[94] X. Wang, N. Wang, H. Ni, Q.-F. An, In situ growth of covalent triazine frameworks membrane on alumina substrate for dye/salt separation, Separation and Purification Technology 280 (2022) 119930. https://doi.org/10.1016/j.seppur.2021.119930.
[95] Z. Liu, X. Deng, L. Lin, R. Qiang, Q. Wang, Q. Cheng, J. Yang, X. Yang, W. Ma, X. Li, M. Xu, C. Wang, Q. Xin, K. Zhao, A tris(hydroxymethyl)aminomethane-

modified polyimide membrane with efficient organic solvent resistant performance and high separation selectivity for dye/salt separation, Desalination 549 (2023) 116325. https://doi.org/10.1016/j.desal.2022.116325.
[96] H. Sun, N.X. Wang, X.T. Li, Q.F. An, Fabrication of MOF derivatives composite membrane via in-situ sulfurization for dye/salt separation, Journal of Membrane Science 645 (2022) 120211. https://doi.org/10.1016/j.memsci.2021.120211.
[97] T.F. Pei, M. Deng, C. Ma, H. Yan, A.M. Zhu, L.Y. Ye, Q.L. Liu, Q.G. Zhang, Loose nanofiltration membranes based on interfacial glutaraldehyde-amine polymerization for fast and highly selective dye/salt separation, Chemical Engineering Journal 450 (2022) 138057. https://doi.org/10.1016/j.cej.2022.138057.
[98] P. Manna, R. Bernstein, R. Kasher, Stepwise synthesis of polyacrylonitrile-supported oligoamide membranes with selective dye–salt separation, Journal of Membrane Science 643 (2022) 120035. https://doi.org/10.1016/j.memsci.2021.120035.
[99] H.S. Wang, Z.Z. He, Q.B. Yang, G.Y. Zeng, Z.M. Yang, S.Y. Pu, Fabrication of 2D/2D composite membrane via combining functionalized MXene and MoS2 nanosheets for dye/salt separation, Journal of Environmental Chemical Engineering 10(5) (2022) 108365. https://doi.org/10.1016/j.jece.2022.108365.
[100] X.Q. Feng, D.C. Liu, H. Ye, D.L. Peng, J. Wang, S.Q. Han, Y.T. Zhang, High-flux polyamide membrane with improved chlorine resistance for efficient dye/salt separation based on a new N-rich amine monomer, Separation and Purification Technology 278 (2022) 119533. https://doi.org/10.1016/j.seppur.2021.119533.